Using Radarsat to Detect and Monitor Stationary Fishing Gear and Aquaculture Gear on the Eastern Gulf of Thailand

by

Catherine Dawn Steckler

Bachelor in Science, University of Victoria, 2001

A Thesis Submitted in Partial Fulfillment of the Requirements for the Degree of

MASTER IN SCIENCE

in the Department of Geography

Supervisor: Dr. K.O. Niemann

Abstract

Stationary fishing gear and aquaculture gear are common sites along the east coast of the Gulf of Thailand. Although these industries provide many people in the region with an income, stationary fishing gear and shellfish culture gear can be destructive to near shore coastal habitats and wild fish populations, which has become a major concern for government fisheries officials in Thailand. The Thai government is looking for cost effective ways to monitor and evaluate these resource activities.

Identifying the number, location and type of stationary fishing and aquaculture gears along the Thai coastlines represents a significant first step in developing a management strategy to monitor this flourishing, resource producing activity. Radar satellite technology may provide a rapid and effective means of surveying and monitoring the spread of these gears in coastal environments, and if proven successful, this approach could potentially be adopted by other coastal resource management agencies in Southeast Asia and other regions of the world.

This thesis focuses on determining if fine beam mode Radarsat-1 imagery can be used to identify the number and location of these stationary fishing and aquaculture gears along the eastern Gulf of Thailand coastline, and also determining if an efficient, automatic signature separation of the gear types is possible. Five multi temporal and multi angle (F2, F4, F5) Radarsat-1 images taken between April and July 2002 were combined to increase the information available for processing and analysis and to determine their gear detection abilities.

Both the stationary fishing gear and aquaculture gears were identifiable on full resolution zooms of the raw satellite imagery, however techniques such as adaptive filtering and image segmentation improved the visual and numerical gear separation. Statistical analysis of the digital number values showed that the different gear types in the study area may be automatically separated using a supervised classification method with 51 % accuracy, whereas the gears as a group can be automatically separated from water segments with an 88% accuracy. Further, with adequate field notes and photographs, manual classification of the different gear types produces high accuracy. Although the gears were identifiable on all images, the shallower angled F4 and F5 images provided more gear information than the steeper angled F2 image. Multi-angle imagery is not necessary for fishing and aquaculture gear detection or separation; however, multitemporal imagery can be useful in detecting gear removal or construction.

Table of Contents

List of Tables

List of Figures

Acknowledgements

For his knowledge and support I would like to thank Dr. Olaf Niemann who supervised me through this research project and countless other remote sensing ventures. Without your trust I couldn't have gained the experiences I have.

I would also like to thank my committee members, Dr. Mark Flaherty, who helped support my field survey in Thailand through the CIDA Tier 2 Project, and Dr. David Goodenough, who offered the use of his lab at the Pacific Forestry Centre for some of my processing work. Your time and effort is greatly appreciated.

Thanks also to Andrew Dyk at the Pacific Forestry Centre for his eCognition discussions and to Dr. Maycira Costa at the University of Victoria for her methodology brainstorm sessions.

Acknowledgements for financial support go to the Canadian Space Agency (CSA), the Canadian International Development Agency (CIDA) Tier 2 Project and the Centre for Asian Pacific Initiatives (CAPI). Without these funding sources the project would not have been possible.

To the people at Burapha University who helped me complete my field study and made my time in Bang Saen enjoyable and rewarding, thank you. Thanks for braving the stormy waters with me Kashane, Surat and Brian!

Special thanks to the Fancy family for providing a most excellent refuge in Bangkok, a fortress in Ang Sila and warm hospitality all around.

To my research companions, Nina Fancy and Michele Moore, thanks for the laughs and support abroad and at home.

Thanks to all of my friends and colleagues who supported me in this endeavor, your humor kept me going.

Special thanks to my parents Edward and Margaret Steckler and to my sister Rhonda and brother Shaun for their love and support through this challenging time and always.

Finally, thank you to my best friend Behrooz Taghan. Thank you for your patience, support and love. *Kheily, kheily mamnoon azizam, berim yek zendegiye jadid shuru konim!*

Dedication

For Kate and Malcolm,
To a bright future and a better world!

Chapter 1

1.0 Introduction

The objective of this chapter is to provide a context and rationale for performing this research, to discuss the objectives of the study and to outline the thesis structure.

1.1 Rationale

Currently, marine and coastal environments provide both renewable and non-renewable resources for human use and development. Concern that future use of these environments may be harmed by increasing resource extraction pressures and overuses of productive areas calls for the development of technologies that may aid in the sustainable management of resource sites. Johannessen *et al.* (1993) stress the need for better monitoring of marine and coastal environments and suggest remote sensing as an option. Remote sensing allows for the rapid acquisition of accurate information from sensitive resource areas and may help provide managers with better tools to make timely decisions where problems exist.

The application of satellite remote sensing technology to natural sciences research provides an efficient way of mapping and monitoring natural systems and resource use (Mumby *et al.*, 1999; Kourti *et al.*, 2001). Ground based studies are often expensive and time consuming so monitoring is performed less frequently, which is less than ideal in a fast changing environment. Numerous remote sensing data sources and compatible computer programs are available to aid in answering management questions today; however, the technology is much more advanced than the application knowledge

(Niemann, 2001). Engineers have developed various types of satellite sensors to detect different characteristics of the earth's surface such as optical sensors, thermal sensors and radar sensors. These sensors collect information about the earth's surface in different manners and provide different views of the surface structure. There remain many satellite imagery applications to be studied in order to determine the full range of usefulness of these satellite remote sensing technologies.

Previous studies in tropical areas have attempted to map land use with satellite imagery from optical sensors; however the environmental conditions do not always allow for clear imagery from these sensors (Pasqualini *et al.*, 1999). Heavy cloud cover throughout the rainy season results in poor image data in the tropics (Corbley, 1995; Forster, 1996; Costa, 2000). The use of data from a radar microwave sensor, Canada's Radarsat-1, may overcome this problem. Radar sensors are all-weather sensors that can penetrate most atmospheric disturbances, such as clouds, rain and haze (Campbell, 1995; Corbley, 1995; Alexander and Inggs, 1996; Costa, 2000) providing a clear view of the earth's surface.

Radar satellite imagery is used both commercially and scientifically in fields such as agriculture, forestry, oceanography, ice studies and coastal monitoring. However, many applications in these fields and others are yet to be studied. This research project will determine the feasibility of using Radarsat's fine beam mode imagery to detect and monitor the distribution of stationary fishing gears and bivalve aquaculture gears in the coastal and near-shore waters of the eastern Gulf of Thailand by assessing the ability to separate the backscatter signatures of small, stationary, near-shore features.

1.2 Goal and Objectives

The goal of this research is to determine if radar remote sensing can be used to detect and separate the spatial patterns associated with small, stationary, near-shore features. The research will be conducted on fine beam mode Radarsat-1 imagery from an area along the eastern coast of the Gulf of Thailand that has a high fishing and aquaculture use. Four research questions are addressed:

1. Can fishing and aquaculture gear composed of bamboo and palm stakes be detected by radar satellite imagery? These gears have structures that protrude above the water surface and should act as corner reflectors on low tide images; however, their filamentous structure may reduce the signal power.
2. Do these different types of gear have distinct spatial or textural patterns that will allow for signature separation? Each of the gears studied has a different structure, shape and location, which, theoretically, should allow for separation.
3. Will a specific incidence angle be better at determining the differences in signal or gear separation? The five images to be analyzed are taken from three different incidence angles of the satellite so may provide different textural pictures. Using a combination of the images to achieve maximum information will be tested.
4. Is multitemporal imagery necessary for the detection and separation of the features of interest? The five images were taken on different dates between April 8th and July 6th, 2002. If the gears are removed or moved over this time period, perhaps multi-date imagery is necessary for this application.

1.3 Thesis Outline

This thesis consists of six chapters. Chapter two describes the status and trends of the coastal fishing and bivalve aquaculture industry on the east coast of the Gulf of Thailand as well as the distribution and structures of the various gear types. This chapter also provides an introduction to remote sensing and, more specifically, radar satellite imagery and describes the possibility of its use as a tool in the detection of coastal fishing and aquaculture gear. Chapter three describes the study area and the data sources used for this research as well as the methodology for collecting the field data. Chapter four outlines the methods of the computer image preprocessing and processing steps and describes some of the processing methods. Chapter five presents the results from the image analysis and discusses the findings of the research. Finally, in chapter six the conclusions and implications of the research are discussed.

Chapter 2

2.0 Remote Sensing as a Tool in Monitoring Coastal Fishing and Aquaculture Gears on the Eastern Gulf of Thailand

This chapter has two main objectives. First, to provide background information on the types of coastal fishing and aquaculture gear located in the study area during the 2002 field season, as well as to describe the actual gear structures and spatial distributions. Second, to give a basic introduction to satellite remote sensing and to discuss the use of remotely sensed radar imagery in the detection and monitoring of the types of stationary, near shore gears in the study area.

2.1 Fishing Gear Status and Trends in Thailand

2.1.1 Thai Fisheries

In many communities fishing is essential not only to nutrition, but also to culture and employment. Fishing communities, therefore, depend on sustainable fisheries and stock renewal. In recent years, uncontrolled exploitation of the sea appears to be the main reason for fish stock collapse in many regions of the world (Pauley *et al.*, 1998); however, growing pollution problems in coastal waters also affect productivity (Suvapepun, 1997). In the Gulf of Thailand the numbers of landed, economically important species have been greatly reduced since 1984 (Bhatiyasevi, 1997). Further, Suvapepun (1997) suggests coastal waters of the Gulf have undergone intensive fishing for the past twenty to thirty years and that demersal fish stocks have shown signs of decline since 1972.

The Department of Fisheries in Thailand realizes this critical resource situation

and has attempted to impose management laws that apply to seasonal closures, gear restrictions, and limited entry to fisheries (SEAFDEC and Kasetsart University, 1997); however enforcement of these measures has been limited. The construction of stationary fishing gear in specific areas has been illegal since 1991, with exception to gears with grandfather rights (Szuster, pers. com., 2001). Regardless of these laws, construction of these fishing devices continues in multi-use estuaries in the Gulf of Thailand and other areas. The Department of Fisheries simply does not have the personnel and equipment needed to monitor and enforce resource management laws (Szuster, pers. com., 2001), and therefore is interested in efficient alternatives for mapping and monitoring estuary use in their country.

2.1.2 Stationary Fishing Gear

The term "stationary fish trap" is used for a variety of large and complex stationary fishing gears in coastal waters less than 20 meters deep (Okawara *et al.*, 1986). The introduction of western trawl fishing to Thailand in 1960 has resulted in fewer stationary fish traps in use today in this region (Chalermwat and Lutz, 1989); however, approximately 25 of these gears were present in the study area between April and July 2002. The main species trapped in this gear type today include mackerel (in the further off-shore traps), anchovy, squid and other uneconomically important fish. These species are sold both for human consumption and to the feed industry (Saraya, 1982).

2.1.3 Coastal Aquaculture Gear

The aquaculture gears existing in the study area include mussel stakes, oyster platforms, blood cockle enclosures and long-line mussel culture. The first three gear types occur in large density mainly in sheltered bays and estuaries, while the long-line gear is new to the area and occurs only at one location in the far south of the study site.

Mussel culture in Thailand is considered more a semi-culture, as the production of both the mussel seed and the food for juvenile and adult mussels is entirely provided by nature (Lutz *et al.*, 1989). In Thailand, two species of mussel are cultured, the green mussel, *Perna viridis*, which is most commonly sold for human consumption, and the striped horse mussel, *Musculus senhauseni*, which is often sold as poultry feed (Saraya, 1982). The green mussel is the most widely cultured in the study area. Initially, mussel aquaculture in Thailand was opportunistic, as mussels were harvested off the abundant stationary fishing traps before fish trawling was introduced (Chalermwat and Lutz, 1989). After the decline of stationary fish trap use, plots of mussel aquaculture were constructed by driving bamboo or palm stakes into the sandy substrate in subtidal areas where mussel settlement naturally occurs (Lutz *et al.*, 1989).

Oyster culture began approximately 50 years ago in Thailand following a decline of natural beds from increased human demands (Brohmanonda *et al.*, 1988). The main species of culture in Chonburi Province is a small oyster *Saccostrea commercialis*, which provides an inexpensive protein source in the region. There are various methods of oyster culture; however, the method used in the study area today is the use of bamboo platforms with hanging ropes for oyster attachment (Brohmanonda *et al.*, 1988). Remnants of the old system of oyster culture remain in Bangsai Bay, where numerous

abandoned cement posts fill the coastline at low tide. The cultured oysters feed naturally from tidal flows of nutrients.

Cockle culture in Thailand began approximately 70 years ago and has a less advanced system than other bivalve culture systems (Saraya, 1982). Cockle seed is simply collected from natural cockle grounds, and then sown on favorable coastal mud flats to be raised to market size (Saraya, 1982).

Long-line culture techniques are new to the study area. In this culture system mussel or oyster spat is collected on hanging ropes below the water surface and grown to adult size for local markets (Vakily, 1989). The long-line gear in the study area is used to cultivate green mussels.

2.2 Structure and Spatial Distribution of Fishing and Aquaculture Gear

2.2.1 Stationary Fishing Gear

Stationary fishing gears, regardless of size or exact shape, are composed of three parts: leaders (guides), playground (sometimes omitted) and codend as seen in Figure 1 (Okawara *et al.*, 1986). The bamboo or palm poles used to construct the gears are approximately 5 to 15 centimeters in diameter and vary from 4.5 to 16 meters long (Chalermwat and Lutz, 1989) depending on the depth of the water. The leaders of gear found in the study area are composed mostly of bamboo stakes and act to guide fish into the trap. They are set into the sandy mud bottom and protrude above the water surface on lower tide levels. The leader density (approximately 15 to 30 centimeter stake spacing) acts as a fence that guides fish into the playground area of the trap. A trap may have 2 to 5 leaders ranging in length from10 to 800 meters (Okawara *et al.*, 1986). The playground

is a c-shaped or triangular enclosure also constructed of bamboo stakes driven into the ocean floor and may or may not be covered with polyethylene netting. The stakes of the playground and the codend protrude approximately 6 to 8 meters above sea level at low tide, whereas the leaders stand about 2 to 3 meters above sea level at low tide and barely breach the surface or are completely submersed at high tide. When the fish exit the playground they enter the codend, which is a semi-elliptical enclosure often covered in netting or chicken wire. Codends in the study site, which are elliptical in shape, varied in diameter from approximately 20 x 30 to 35 x 50 meters. The funnel shaped entrance to the codend prevents the fish from escaping this area and the fisherman can bring a small boat into the trap and collect the fish. Alternatively, some of these gear types have a removable bag net so fish can be hauled away rather than collected on site (Okawara *et al.*, 1986).

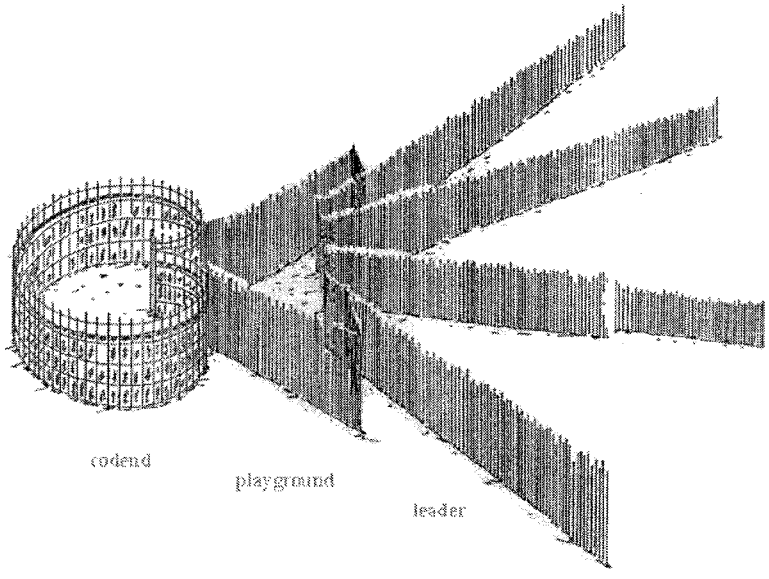

Figure 1 Typical stationary fish trap design on the Eastern Gulf of Thailand (modified from Okawara *et al.*, 1986)

Bamboo stake traps are usually built so that the main leader, which is the longest one, faces toward shore and the opening to the trap faces the current at ebb tide (Okawara *et al.*, 1986). In this way, fish are brought to the leaders with the outgoing tide and captured in the trap. Typical stationary fishing gear in the study area can be seen in Figures 2 and 3 below.

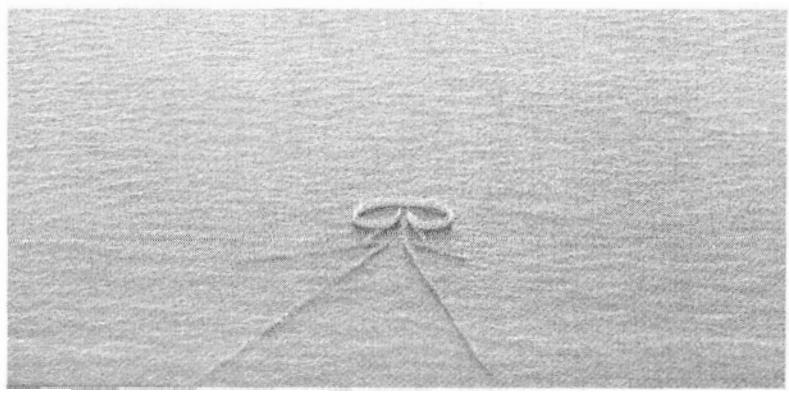

Figure 2 Aerial view of stationary fishing gear near Bang Saen, Thailand

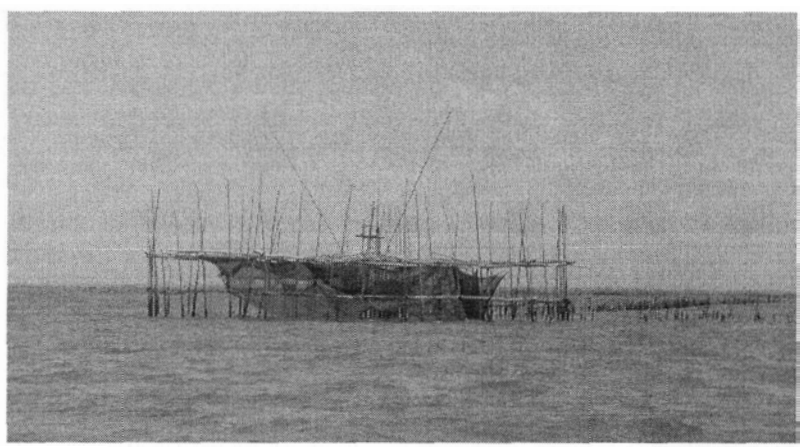

Figure 3 Ground view of stationary fishing gear near Bang Saen, Thailand

2.2.2 Mussel Stakes

Mussel culture gear is more basic than that used for fish traps. Bamboo or palm poles are set into the substrate in long rectangular clusters where poles are approximately 0.5 to 1 meter apart and gear clusters are 4 to 8 poles wide by 20 to 200 meters long (Lutz

et al., 1989). Harvest navigation lanes of 8 to 10 meters separate the gear clusters from one another (Lutz *et al.*, 1989). From an aerial view, the mussel gears appear to be long, irregular rectangles of dense bamboo stakes as seen below in Figure 4. Figure 5 gives a close-up view of a section of mussel stake clusters.

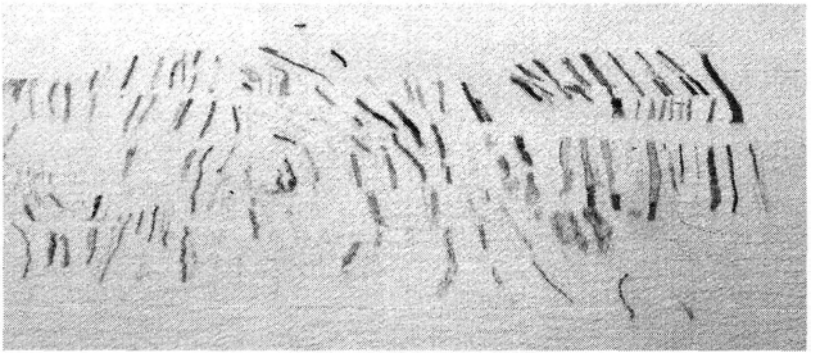

Figure 4 Aerial view of green mussel stake farms near Bang Saen, Thailand

Figure 5 Ground view of mussel stakes near Bang Saen, Thailand

2.2.3 Oyster Platforms

There are numerous methods for oyster culture ranging from simple to complex in structure. The platform method used today in the study area is more complex and is often termed hanging culture. Bamboo stakes are used to construct sturdy, rectangular platforms from which ropes hang vertically into the water. Platforms stand approximately 2 meters above the water surface at low tide and are generally 3 to 4

meters wide and 10 to 50 meters long. As seen in Figure 6, the platform structure is fairly dense in comparison to the mussel gear structure. Figures 7 and 8 show a close-up view of oysters hanging from platforms at low tide.

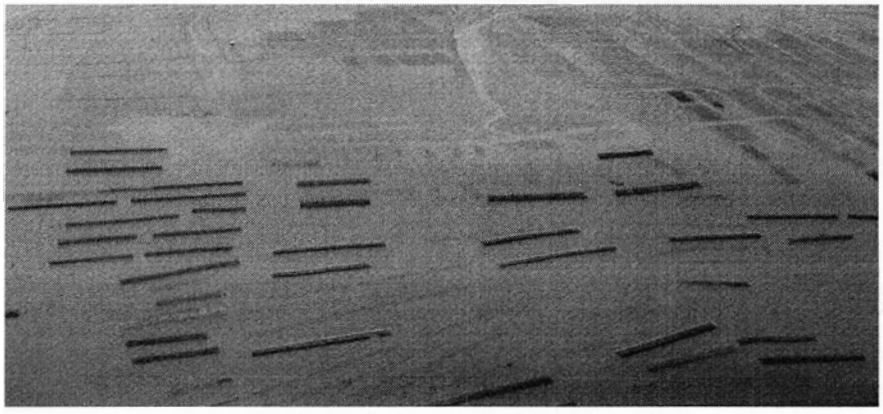

Figure 6 Aerial view of oyster platforms in coastal zone near Ang Sila, Thailand

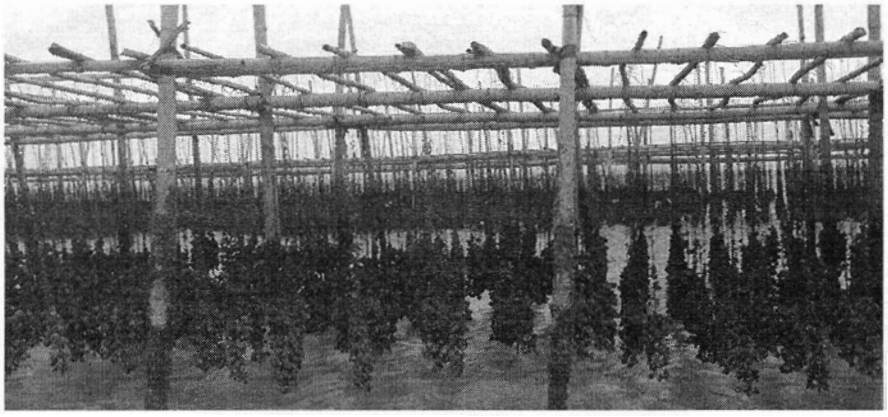

Figure 7 Ground view of oyster platform at low tide near Ang Sila, Thailand

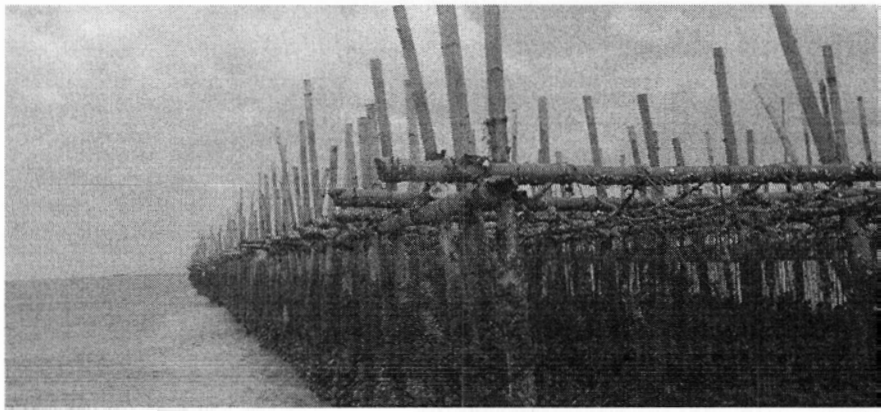

Figure 8 Lengthwise view of same oyster platform as in Figure 7

2.2.4 Blood Cockle Enclosures

Blood cockle farms consist of a fence built by driving bamboo stakes approximately 50 centimeters in length into the mud to form individual plots with approximately 20 to 30 centimeter stake spacing (Saraya, 1982). Cockle farms in the area are generally 1 to 5 hectares for family run operations and 30 to 100 hectares for commercial farms (Saraya, 1982). Figure 9 shows an aerial view of numerous blood cockle enclosures. In Figure 10 a ground view of cockle enclosures displays the simple structure.

Figure 9 Aerial view of blood cockle enclosures constructed from bamboo poles near Chonburi, Thailand

Figure 10 Ground view of blood cockle enclosures near Chonburi, Thailand

2.2.5 Long-line Mussel Culture

Long-line culture systems consist of ropes, or wooden rafts with ropes attached, which are suspended below the water surface from floating devices (Saraya, 1982) such as empty gasoline barrels painted with anti-rust agents (Brohmanonda, 1988). The gears in the study area are simple rafts, often joined by ropes with floatation devices (barrels). These rafts have many ropes hanging vertically into the water and are kept stationary with anchors. The rafts in the study area are not completely submerged, but otherwise are similar to the type shown in Figure 11. Figure 12 gives an aerial view of long-line gear near Siracha shows the structure of gear in the study area.

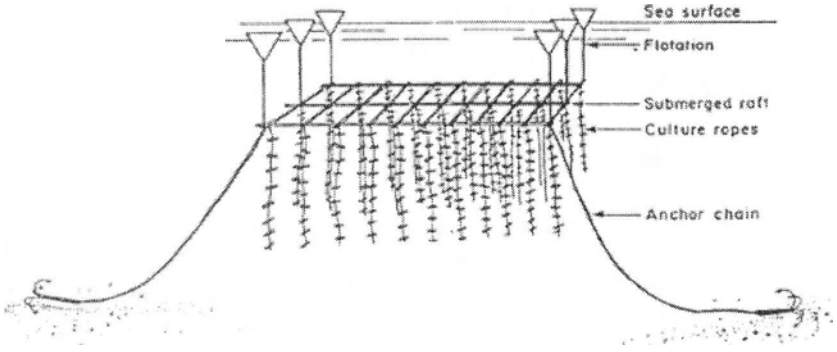

Figure 11 Diagram of submerged long-line raft mussel culture gear (Vakily, 1989)

Figure 12 Aerial view of long-line mussel gear near Siracha, Thailand

2.3 Digital Remote Sensing

According to Lillesand and Kiefer (2000), "remote sensing is the science and art of obtaining information about an object, area, or phenomenon through the analysis of data acquired by a device that is not in contact with the object, area, or phenomenon under investigation." In the case of radar digital data, information is acquired via aircraft or satellite using sensors that record the signal backscatter data as image pixels, each pixel having a digital number value (DN value) corresponding to the backscatter signal's phase and amplitude. Electromagnetic energy creates the data image, whether dealing with visible, infrared, heat, microwave or radio forms of energy (Lillesand and Kiefer, 2000). The spectrum below in Figure 13 displays the wavelength at which each energy type dominates. In the case of this research microwave energy with a 5.6 centimeter wavelength was used to test its ability to detect small, stationary fishing and aquaculture gears in coastal waters.

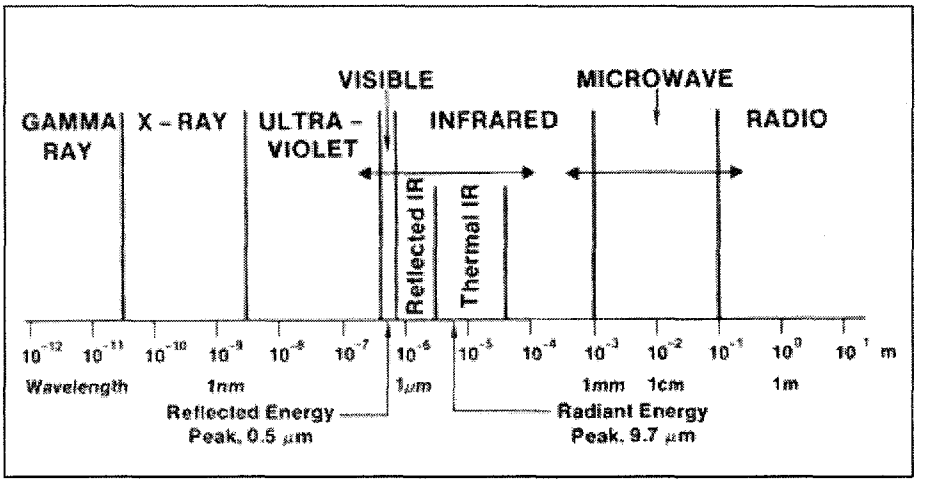

Figure 13 Diagram of the electromagnetic spectrum (modified from Sabins, 1997, p.4)

When electromagnetic energy comes in contact with the earth's surface or objects on the earth's surface, it will be reflected, absorbed or transmitted by that object

(Lillesand and Kiefer, 2000). These three energy interactions together describe the incidence (incoming) energy (Equation 1) (Lillesand and Kiefer, 2000).

Incidence Energy	$E_I(\lambda) = E_R(\lambda) + E_A(\lambda) + E_T(\lambda)$	Equation 1

Where:

E_I = incidence energy
E_R = reflected energy
E_A = absorbed energy
E_T = transmitted energy

The above energy balance equation describes the relationship between reflection, absorption and transmission; however, reflected energy is the energy of interest in remote sensing as reflected energy predominates in the wavelengths used by these systems (Lillesand and Kiefer, 2000). Equation 2 describes how reflected energy is equal to the incidence energy on a feature minus the energy that is absorbed or transmitted by that same feature (Lillesand and Kiefer, 2000).

Reflected Energy	$E_R(\lambda) = E_I(\lambda) - [E_A(\lambda) + E_T(\lambda)]$	Equation 2

Where:

E_R = reflected energy
E_I = incidence energy
E_A = absorbed energy
E_T = transmitted energy

A given surface or object (reflector) will create a signal that is made up of a unique combination of these three energy interactions, which allows the distinction between different features or surfaces in an image (Lillesand and Kiefer, 2000). The

geometry of the energy reflected from an object also affects the signal strength. Reflectors will result in some level of diffuse or specular reflection. Diffuse reflectors are rougher surfaces that reflect energy in all directions, while specular reflectors are smoother surfaces that behave like mirrors, where the angle of reflection equals the angle of incidence (Lillesand and Kiefer, 2000). Figure 14 describes the various scenarios of energy reflection off different surface types.

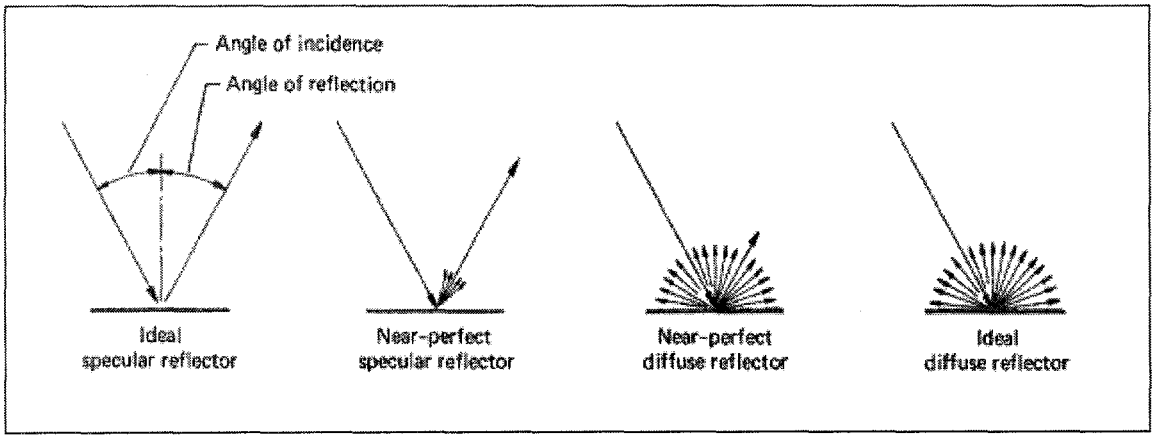

Figure 14 Different energy reflection scenarios (Lillesand and Kiefer, 2000, p. 13)

Not only the surface character, but also the wavelength of the incoming energy dictates the reflector type a given surface will act as. For example, with a relatively long microwave wavelength a sandy beach can appear smooth to the incidence energy, whereas with a shorter wavelength from the visible spectrum it will appear rough (Lillesand and Kiefer, 2000). This occurs because the larger microwave wavelengths do not interact with the relatively small ripple features of the sand grains that give a beach its textural pattern and so very little energy will be returned to the sensor to be recorded, whereas the significantly smaller wavelengths of the visible spectrum interact with the textural variation of the small sand features and a significant amount of energy is received by the sensor, resulting in a distinct pattern being recorded. In the case of this

study, the 5.6 centimeter wavelengths will interact with the 5 to 15 centimeter diameter bamboo poles, sending significant backscatter information back to the sensor. The similarity in size of the energy wavelength and the feature of interest results in increased energy interaction and therefore increased return radar signals, which creates the textural patterns.

2.4 Radar Systems

Radar satellite images differ from images from optical sensors or aerial photographs in that they represent the textural patterns of the surface being detected. The surface interacts with the microwave energy, and depending on the surface's configuration and the radar energy wavelength, returns a signal to the satellite sensor. The radar image created from this process is often a single band, monochromatic representation of the earth's surface, rather than a multi-band, colour image of the earth that an optical sensor would produce, although multi-band radars do exist. In an 8-bit radar image, a pixel digital number value of 0 corresponds to a pure black pixel and a value of 255 would be a pure white pixel.

One of the biggest advantages of radar sensors is that they do not rely on the sun's energy to image a surface as passive sensors do; they instead are active sensors that utilize their own microwave energy in the longer wavelength portion of the electromagnetic spectrum. This has two advantages:

1. The sensor can be active 24 hours a day providing more imaging times as the satellite is providing its own energy source and does not rely on sunlight for illumination.

2. Using microwave energy means that the sensor can penetrate most cloud, haze and rain because of the longer wavelengths. This allows for higher quality and more consistent imaging.

2.4.1 Wavelength

Radar remote sensing systems are active systems that release their own energy source of microwave pulses to interact with the surface to be sensed, this surface then returns a signal back to the sensor where its backscatter strength is recorded. Microwave energy, like other energy forms, follows the basic wave theory as it travels through space (Lillesand and Kiefer, 2000). The energy moves in a rhythmic, sinusoidal pattern at the velocity of light, where the distance between one wave peak and the next is the energy's wavelength (λ) and the number of peaks passing a given point in space over a set amount of time is the waves frequency (ν) (Lillesand and Kiefer, 2000). Electromagnetic energy of wavelengths from approximately 1 millimeter to 1 meter is considered microwave energy and has only been applied by civilians in the geosciences since the 1960s (Henderson and Lewis, 1998).

Imaging radar satellites operate at one specific wavelength or frequency (Henderson and Lewis, 1998), thereby creating different textural pictures of surface features depending on the wavelength used. Table 1 describes the satellite wavelength bands used in remote sensing and expresses the wavelength and frequency range of each band.

Table 1 Imaging radar satellite wavelengths and frequencies (Sabins, 1987, p.180)

Band Designation	Wavelength (λ), cm	Frequency (v), GHz
K	0.8 to 2.4	40.0 to 12.5
X	2.4 to 3.8	12.5 to 8.0
C	3.8 to 7.5	8.0 to 4.0
S	7.5 to 15.0	4.0 to 2.0
L	15.0 to 30.0	2.0 to 1.0
P	30.0 to 100.0	1.0 to 0.3

Each energy wavelength will interact differently with given features on the ground to produce different images as seen in Figure 15. The top image (C-band) clearly shows a different view of the agriculture crops than the lower (L-band) image. This difference results from the different way in which a 5 centimeter wavelength will interact with the crop's components compared to a 20 centimeter wavelength.

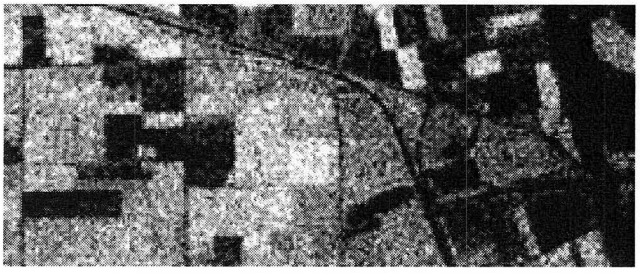

(a)

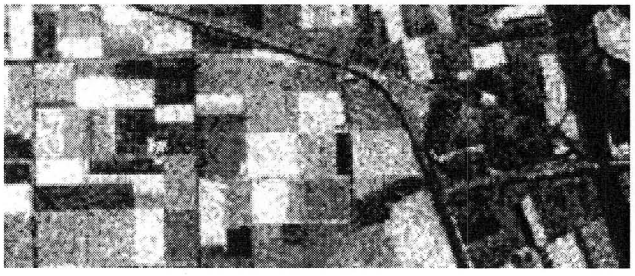

(b)

Figure 15 Radar images of the same agricultural fields. Image (a) was created from a C-band sensor, while image (b) was collected from an L-band sensor (CCRS, 2001)

2.4.2 Incidence Angle

The incidence angle is the angle between the transmitted radar beam and a vertical line perpendicular to the surface (Sabins, 1997; Lillesand and Kiefer, 2000) as

seen below in Figure 16. In general, the total amount of signal backscatter increases as the incidence angle decreases or becomes steeper (Fung and Ulaby, 1983). Fung and Ulaby (1983) suggest that imagery with a steeper incidence angle will be brighter than imagery with a shallower angle because a greater amount of the radar backscatter signal is returned to the sensor. For example, with Radarsat-1 imagery, an image acquired from the F1 or F2 incidence angle (steep) will often create an overall brighter signal than an image acquired from the F4 or F5 angle (shallow). This occurs due to the geometry of the surface to the sensor as well as the scattering properties of the surface and is intrinsic in multi-angle radar imagery.

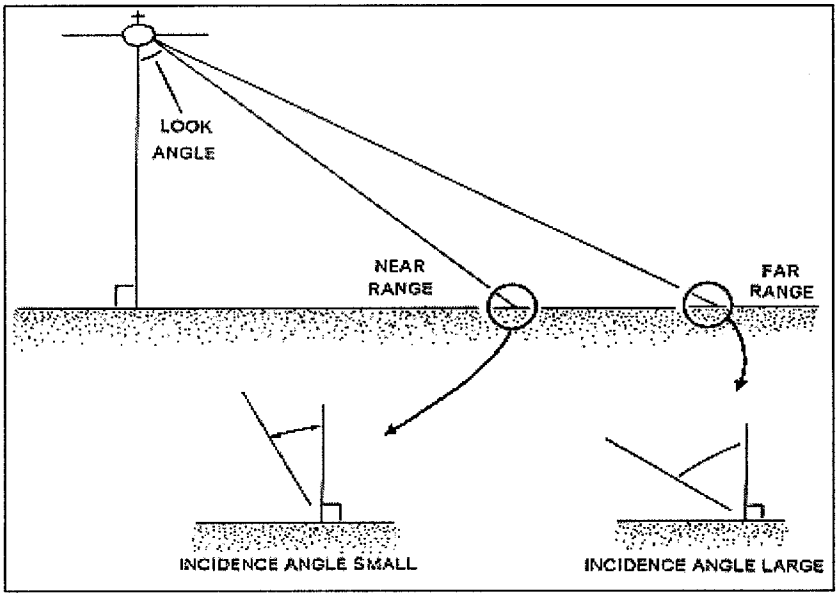

Figure 16 The near range of the image swath width has a steeper incidence angle than the far range because the angle of the incidence energy from normal to the surface increases as you move away from the sensor (Campbell, 1987)

2.4.3 Polarization

The polarization of a satellite describes the orientation of both the transmitted and received electromagnetic wave energy. Nonpolarized energy vibrates in all directions perpendicular to the direction in which the energy travels (Jensen, 2000). However, with

polarimetric radar systems the signal pulses can be filtered so that the electrical waves vibrate in a single plane perpendicular to the direction of wave propagation (Lillesand and Kiefer, 2000). Both incoming and outgoing waves may have either horizontal or vertical polarization, which leads to the following polarization scenarios:

Like-Polarized -	HH – horizontal transmission, horizontal reception
	VV – vertical transmission, vertical reception
Cross-Polarized -	HV – horizontal transmission, vertical reception
	VH – vertical transmission, horizontal reception

As Henderson and Lewis (1998) explain, a wave's polarization affects how it interacts with the structure of features on the ground, therefore radar imagery collected using different polarization and wavelength combinations may result in different and complementary information about the objects being detected. In general, like-polarized imagery will return a greater signal than cross-polarized imagery because only the depolarized part of the signal will be returned to the sensor (Henderson and Lewis, 1998).

2.5 Radarsat-1 and Gear Detection

2.5.1Radarsat-1 Characteristics

Radarsat-1 is an imaging radar satellite that was launched on November 4, 1995 by the Canadian Space Agency and holds a synthetic aperture radar (SAR) imaging instrument (CCRS, 2001; Henderson and Lewis, 1998). This satellite has a polar, sun-synchronous orbit with a 24 day repeat cycle (CCRS, 2001). Radarsat-1 is a single frequency C-band (5.6 cm wavelength), horizontally polarized (HH) sensor with the ability to operate in seven different beam modes (CCRS, 2001). These unique beam modes can provide imagery ranging from approximately 45 to 500 kilometer swath

widths, 8 to 100 meter resolution and incidence angles from 20 to 60 degrees, as seen below in Figure 17 and Table 2 (CCRS, 2001).

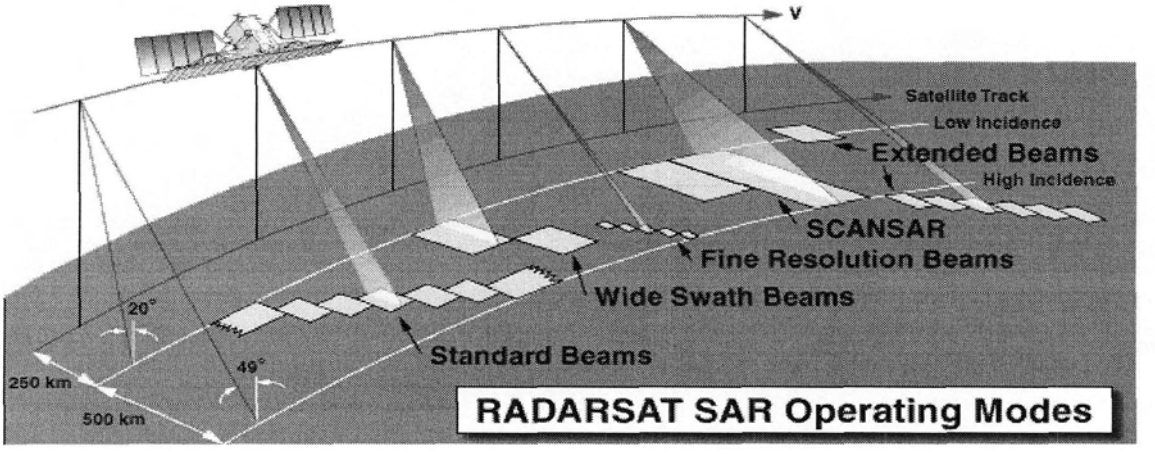

Figure 17 Radarsat-1 SAR operating modes (CCRS, 2001)

Table 2 Radarsat-1 imaging beam mode characteristics (CCRS, 2001; Henderson and Lewis, 1998)

Beam mode	Approx. resolution (m)	Swath width (km)	Incidence angle (°)	Number of looks
Standard	25	100	20 – 49	4
Wide 1	30	165	20 – 31	4
Wide 2	30	150	31 – 39	4
Fine resolution	8-10	45	37 – 48	1
ScanSAR narrow	50	305	20 – 40	2 – 4
ScanSAR wide	100	510	20 – 49	4 – 8
Extended high	25	75	50 – 60	4
Extended low	35	170	10 – 23	4

2.5.2 Gear Detection

This project uses five Radarsat-1 images from the fine resolution beam mode because the relatively small size of the materials used to construct the fishing and aquaculture gear would not be detectable on imagery of lower resolution. From image analysis, the approximate 8 meter resolution image data captures enough ground information from the study site to identify the fishing and aquaculture gears, and to some

extent, to visually separate the various gear types according to their physical construction as mentioned earlier. Table 3 shows the near and far incidence angles for each of the fine resolution beam modes of Radarsat. The image data used in this project were acquired with incidence angles F2, F4 and F5 to test the difference between steep and shallow angles for detection of the coastal gears.

Table 3 Beam positions of fine resolution mode (CCRS, 2001)

Beam Number	Incidence Angle (°) (near range)	Incidence Angle (°) (far range)
F1	36.9	40.1
F2	39.3	42.3
F3	41.6	44.2
F4	43.6	46.0
F5	45.3	47.8

Few radar satellite imagery based studies have attempted to detect relatively small, man-made structures in the coastal environment. Recently, Hogda and Malnes (2002) found Radarsat fine beam mode imagery (F5) successful at detecting circular fish cages that breach the water surface in Norway's coastal waters. All of the metal cages in the study area were clearly defined and cages constructed from polymer rings with diameters of 20 meters were also detectable after filter processing. Related radar studies looking at ship detection have been successful, however these ships are large, solid, metallic structures, whereas stationary aquaculture and fishing gears are constructed mainly from wood and netting, and have a filamentous and patchy structure and distribution. These near-shore features breach the water surface creating dihedral (corner) reflectors as seen in Figure 18, which should aid in their detection. The corner reflector scenario results when an object perpendicular to the surface intercepts the

energy being specularly reflected from a smooth surface and reflects this energy back to the sensor. If many of these signals come in contact with the corner reflector object, then a relatively strong signal is produced on the image resulting from the increased energy return.

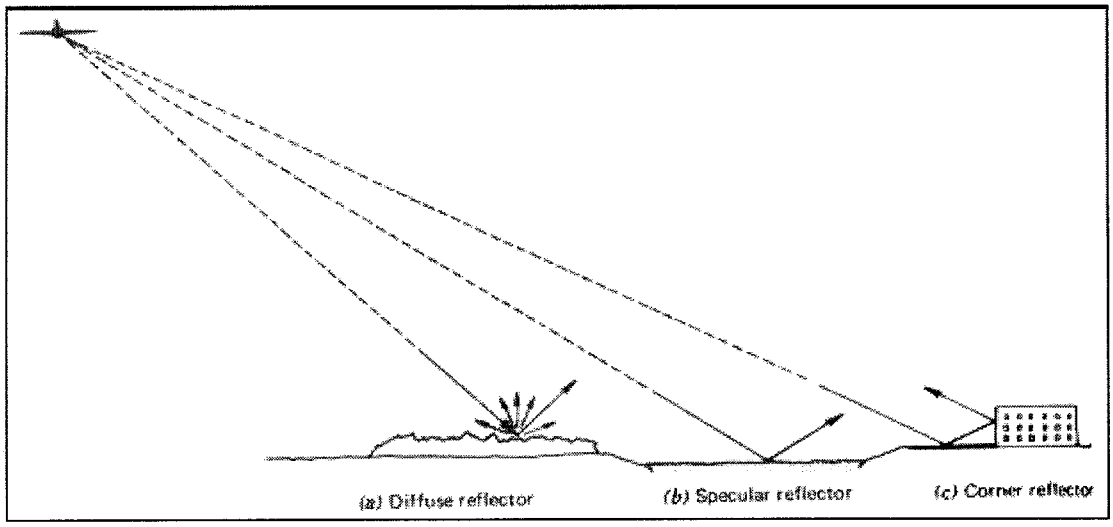

Figure 18 Radar reflection from different surface types (Lillesand and Kiefer, 1987, p.496)

2.5.3 Seven Factors That Will Aid in Detection of Fishing and Aquaculture Gear

There are seven main factors that should enable the different gear types to be detected and possibly separated using Radarsat-1 satellite imagery. Five of these factors have already been discussed and are related to the choice of Radarsat-1 imagery for the project. These include the fact that Radarsat-1 is an active sensor, so imagery can be acquired at the best possible time to coincide with the appropriate tide levels on a 24-hour basis. Also, the presence of clouds or rain at the imaging time should not degrade image quality, as the microwaves will penetrate such atmospheric disturbances. Secondly, the ability to view the scene from different incidence angles will increase the amount of backscatter information available to be tested. Thirdly, using a C-band sensor such as

Radarsat-1 provides wavelengths of approximately 5.6 centimeters, which will interact with the approximate 15 centimeter diameter bamboo stakes used to construct the gears. Further, the HH polarization should increase the amount of energy backscatter the sensor receives because the energy's orientation will interact with the fairly dense gear structures that protrude from the water surface. Fifth, Radarsat's fine resolution beam mode produces imagery with approximately 8 meter pixel resolution, which should capture the different gears' dimensions. For example, 3 or 4 image pixels on a raw image would represent the 30 meter diameter fishing gear codends.

The sixth factor deals with the geometry of the gears themselves. As briefly mentioned in section 2.5.2, above water corner reflectors (bamboo stakes) should create bright pixels in the image, which will be surrounded by darker water pixels, as microwave energy is specularly reflected by relatively smooth water surfaces (Gower and Skey, 2000; Jiang, *et al.*, 2000; Wackerman, *et al.*, 2000). With relatively calm seas, the water acts as a specular reflector so that incoming energy is reflected away from the sensor at an incidence angle equal to the incoming angle. In this case, no backscatter signal is returned to the sensor and water pixels appear dark grey to black. The gear, as corner reflector, is affected by the sea state. In calm sea conditions the energy that contacts the gears will be specularly reflected back towards the sensor resulting in a high backscatter signal and bright (light grey to white) pixels. However, if seas are rough, the energy will be diffusely reflected in all directions with only a fraction of the energy returning to the sensor. This last scenario results in a lower return signal, which leads to lower DN pixel values and more difficult gear detection. In order for the gears to be effective corner reflectors they must protrude above the sea surface enough to allow

energy interaction. For this reason, image acquisition must coincide with low tide levels, as many of the aquaculture gears in the region are totally submersed in water at high tide.

Finally, the dielectric constant of the object being detected can affect the strength of the return signal. The dielectric constant is the objects ability to conduct electrical energy (Jensen, 2000). Dry, natural materials have low dielectric constants in the range of 3 to 8, whereas water (or water-saturated materials) has a value of approximately 80 (Jensen, 2000). For this reason, the moisture content of an object can greatly increase the amount of backscatter returned to the sensor. The fishing and aquaculture gears in the study area are saturated with water as they are constructed from woody bamboo and palm stakes and are continuously absorbing water from the sea.

2.6 Summary

The gear types in the study area are typical of the coastal zones throughout the Gulf of Thailand. The study area contains two sheltered estuaries with very high density aquaculture and fishing gear. The larger of these two areas will be the focus of much of the thesis work and image processing, as it contains the three main gear types, excepting the blood cockle and long-line gear.

As the field photographs show, each gear type has a very specific structure and shape, which may allow for the separation of the gears on the radar imagery. The test will be to see if the different structures alter the radar backscatter signals enough to allow consistent, automatic separation of the gear types by applying segmentation or classification algorithms.

Digital remote sensing is well suited to detecting and monitoring the spatial and temporal distributions of different resource uses. The aim of this project is to assess the

use of remote sensing, specifically Radarsat-1 data, as a tool for detecting and monitoring the distribution of stationary fishing and aquaculture gears in the Gulf of Thailand. Radarsat-1 is an active senor that images the earth's surface by generating its own illumination of the scene, (CCRS, 2001). This principle allows Radarsat-1 to record data on a 24 hour basis. Radarsat-1 microwave energy can also penetrate through heavy clouds, dust, haze, and rain because the longer wavelengths of microwave energy do not interact with small atmospheric particles. For this reason, Radarsat-1 imagery is an appropriate choice for this project as the tropical climate of Thailand often results in heavy cloud and rain throughout the wet season. Finally, the choice of multiple incidence angles is an advantage of Radarsat-1 for this project. The multi-angle imagery will allow us to determine the best gear detection results possible. Radarsat-1 SAR imagery may be a useful tool for identifying and separating fishing and aquaculture gear in the Gulf of Thailand.

Chapter 3

3.0 Study Area and Data

This chapter describes the study area selected for this project, discusses the different sources of data used throughout the project, and describes the field research methodology.

3.1 Description of the Study Area

Thailand is located in central Southeast Asia at the approximate coordinates of 15° 00' N and 100° 00' E with the Andaman Sea to the west and the Gulf of Thailand to the east. The country has a total area of 514,000 square kilometers and 3,219 kilometers of coastline (CIA World Fact Book, 2003). As seen in Figure 19, Thailand borders Malaysia to the south and Burma, Laos and Cambodia to the west, north and east.

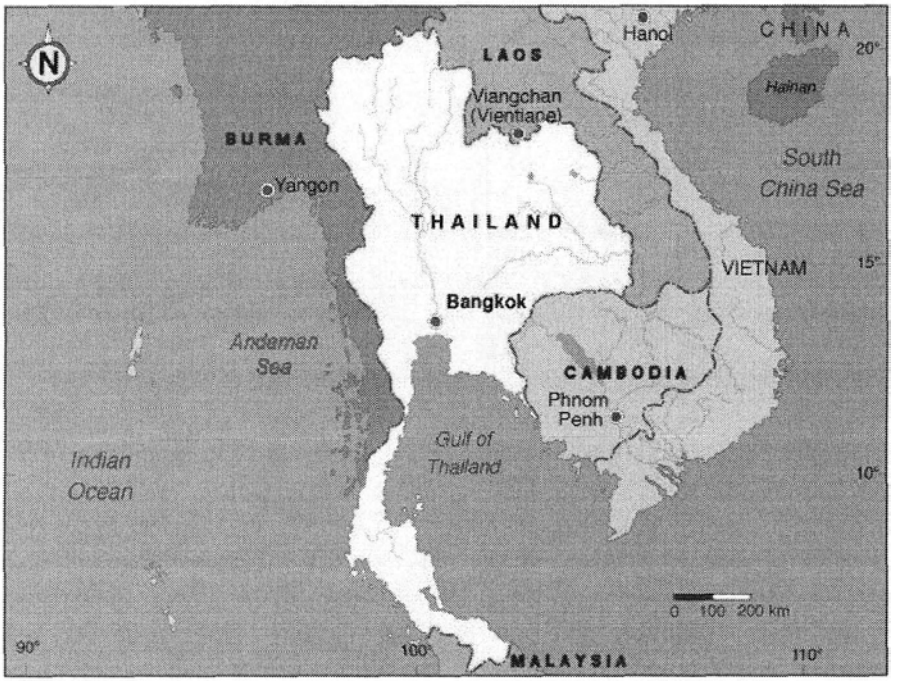

Figure 19 General map of Thailand in Southeast Asia (modified from Maps.com, 2003)

The five Radarsat images acquired for this project cover a small portion of the coastal zone in the upper, eastern Gulf of Thailand just southeast of Bangkok. Field surveys were conducted in the coastal waters up to 10 kilometers from shore at an upper left location of 13°25'00"N / 100°40'00"W and lower right location of 13°10'00"N / 100°58'00"W. The ellipse in Figure 20 outlines the location of the general study area in the coastal waters west of the province of Chon Buri. The satellite imagery was also subset to cover this approximate region to focus on the dense fishing and aquaculture gears found here.

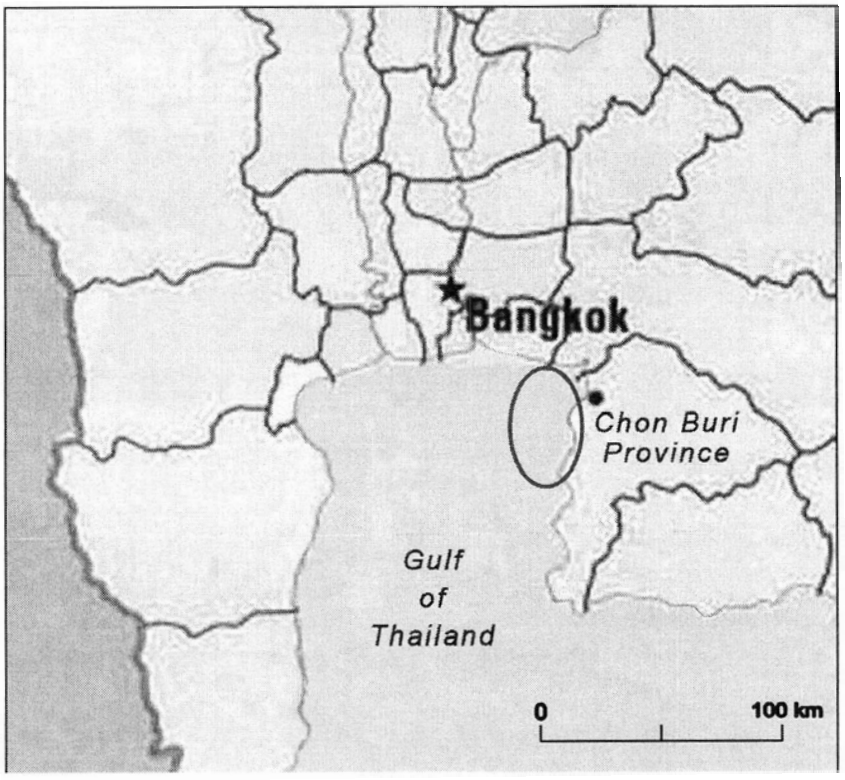

Figure 20 Larger scale map showing the Gulf of Thailand and the study area in the ellipse (modified from Oddens, 2003)

The coastal waters in the upper gulf are fairly shallow at a maximum depth of approximately 10 meters (Royal Thai Survey Department, 1987) and the approximate

daily tidal range in the summer months is 3 meters difference between low and high tide (Hydrographic Department, Royal Thai Navy, 2002). Water quality in the Gulf of Thailand is considered safe, with the exception of more polluted areas near river mouths (Suvapepun, 1997). However, in recent years nutrient levels in coastal areas have increased as a result of increasing inputs from domestic waste, coastal aquaculture effluents, and food processing plant discharges (Suvapepun, 1997). The study area has many land-uses including urban, commercial fishing, small-scale fishing, aquaculture (shrimp, bivalves and fish) and tourism/recreation.

3.2 Data Sources

3.2.1 Acquisition of Radarsat-1 SAR Data

Five Radarsat-1 images with Path Image Plus processing were acquired with the satellites on-board recorder and calibrated by Radarsat International (RSI) in Vancouver, Canada. Images were downloaded from over the study area on five separate dates during the summer of 2002 at three different incidence angles (F2, F4 and F5). Data download timing coincided with field study days and low tides to improve gear detection accuracy. As mentioned earlier, low tide imagery reveals maximum above water gear structures. Major characteristics of the five images are laid out below in Table 4.

Table 4 Characteristics of project Radarsat-1 imagery

Acquisition date	Incidence angle (°)	Coverage (km)	Swath mode	Band polarization	Pixel spacing (m)	Pixel resolution (m)	Number of looks
04-08-2002	45.3-47.8	50x50	F5	C/HH	3.125	8	1
05-17-2002	43.6-46.0	50x50	F4	C/HH	3.125	8	1
05-26-2002	45.3-47.8	50x50	F5	C/HH	3.125	8	1
06-10-2002	43.6-46.0	50x50	F4	C/HH	3.125	8	1
07-06-2002	39.3-42.3	50x50	F2	C/HH	3.125	9	1

3.2.2 Ancillary Data

Ancillary data that contributed to this project includes topographic maps, tide tables, Aster imagery, photographs, GPS data and field notes. All of these data were important tools for finishing this project. The topographic maps of the study area were provided by the Royal Thai Survey Department and used in the field campaign to mark sample sites as data was collected. Current tide tables for the region provided by the Hydrographic Department of the Royal Thai Navy were helpful in ordering the Radarsat-1 imagery to ensure the best possible gear detection data. Aster imagery of the study area from NASA's Terra satellite was used to geometrically correct the Radarsat imagery. The Aster imagery is optical data with 15 meter pixel resolution. Further, the collection of field notes, aerial and ground photographs and GPS positions of the fishing and aquaculture gears in the study area helped to describe the gears being studied.

3.2.3 GPS and Air Photograph Acquisition

Six days between April and July 2002 were spent on the water in a small boat collecting GPS locations, photographs and descriptive information on the types of gear in

the study area. These data were collected to serve as a ground truth for positive identification of fishing and aquaculture gears on the satellite imagery. The GPS used was a Garmin Etrex, with sightings accurate to within ± 8 meters. The study area was also viewed and photographed from a Cessna 172 to better understand the spatial distributions and shapes of the various gears from above. GPS data collection tables are included in Appendix I.

3.3 Field Methodology

Field methods involved identifying the location, size, shape and types of fishing and aquaculture gears within the study area during the summer months of 2002. The study area was surveyed by land, boat and air, and GPS locations of gear samples were documented. Photographs of the different gear types were taken both on the water and from aircraft to further describe the data. This information was compared to backscatter brightness in the satellite images taken during the field campaign to determine if positive identification of gears was possible. A Thai Master's of Science student from the Aquatic Sciences Department at Burapha University and a local man with a boat accompanied me on the boat surveys.

3.4 Summary

Five multi-temporal and multi-angle Radarsat-1 images of the eastern Gulf of Thailand were acquired during low tide levels in order to attempt the detection and separation of three different types of stationary fishing and aquaculture gears in the area. This study area was chosen because it contains two dense regions of the gears and was easily accessed from Burapha University, Bang Saen, Thailand.

Chapter 4

4.0 Methodology

This chapter describes the methods used to complete this project and provides some background information for the image processing techniques tested. Methods discussed include image preprocessing techniques such as radiometric and geometric correction, image subsetting, speckle filtering and image scaling, as well as image processing techniques regarding image segmentation and classification. These methods were performed using PCI Geomatica modules *GCPWorks*, *ImageWorks* and *Xpace* and Definiens Imaging *eCognition* and will assess the ability of using Radarsat satellite imagery to detect and separate the different types of fishing and aquaculture gear in the study area.

4.1 Image Preprocessing

4.1.1 Radiometric Correction

When satellite image sensors record data radiometric errors occur, which alter the true scene backscatter values. Image pre-processing methods may correct these errors, allowing more accurate image digital number analysis. The first radiometric pre-processing step to run on Radarsat imagery is performed by the supplier, in this case, Radarsat International. This image radiometric calibration step creates an image with digital numbers that are true estimates of scene backscatter and is necessary to compensate for changes in scene illumination, atmospheric conditions and imaging instrument characteristics (Lillesand and Kiefer, 1994; Jensen, 1996; Henderson and

Lewis, 1998; Richards and Jia, 1999). The 16-bit calibrated image received has backscatter estimate (sigma, σ) values in intensity units. In order to optimize utilization of the dynamic range of data values and render the multi-temporal images comparable, PCI Geomatica was used to normalize the data by applying a transform to change values from intensity backscatter units to amplitude backscatter units, ultimately creating a 32-bit image that more accurately represents the original radar signals. Amplitude data is the square root of the intensity (power) data format. The first step in this process is to run CDSAR, which reads the Radarsat imagery file in the original format and automatically creates a PCIDSK file. CDSAR reads all of the imagery channels from CD and saves the satellite path information in a file segment (PCI Geomatica, 2000). Next, SARINCD creates a table of incidence angles that relates to the gain scaling values. The image file now contains an orbit segment and array segment (ordered segment for the incident angle tables) required for input for the final step. Finally, SARSIGM produces a calibrated radar backscatter image from the input scaled radar data and an array of incidence angles created in the previous step (PCI Geomatica, 2000). The type of pixel values; intensity, amplitude or decibel, is chosen in this final step to determine the data range desired (Equations 3, 4, 5).

Intensity	$Sigmaij = \frac{DN * DN + A0}{Aj} * \sin(ij)$	Equation 3
Amplitude	$Sigmaij = \sqrt{\frac{DN * DN + A0}{Aj} * \sin(ij)}$	Equation 4
Decibel	$Sigmaij = 10 * \log_{10}\left(\frac{DN * DN + A0}{Aj} * \sin(ij)\right)$	Equation 5

Where:

Sigmaij:	output backscatter coefficient for scanline i, pixel j
$\log_{10}(\ )$:	logarithm base 10 function
$\sqrt{(\ )}$:	square root function
DN:	input image value for scanline i, pixel j
A0:	gain offset from the first member of A0SEG
Aj:	expanded gain scaling table value for column j
sin( ):	sine trigonometric function
ij:	expanded incidence angle table value for column j

I chose to radiometrically correct my data to 32 bit amplitude images, which is the square root of the radar backscatter values and produces a positive range of digital number values (PCI Geomatica, 2000). PCI Geomatica (2000) suggests amplitude as the best option when further image processing such as filtering and classification are to be performed. Amplitude values are preferred because they are the square root of the intensity values so are positive whole numbers and can be averaged successfully, whereas decibel values are on a logarithmic scale and may be positive or negative values so would not result in correct mathematical results when averaging with filters or classification algorithms.

4.1.2 Geometric Correction

Raw digital images are not linked to a coordinate system, but are referenced by their pixel and line coordinates. These images cannot be used as geometrically referenced maps because they have distortions caused by variations in sensor factors such as altitude, attitude and sensor platform velocity, as well as earth rotation and curvature, and relief displacement (Lillesand and Kiefer, 1994, 528p). Two types of geometric distortions, systemic and random, must be corrected. Applying mathematical models to imagery easily rectifies systemic distortions, such as those caused by the eastward

rotation of the earth (Lillesand and Kiefer, 1994, 528p; Jensen, 1996, 107p). The imagery supplier rectifies imagery for systemic distortions. However the random distortions, from sources such as altitude and attitude of the sensor platform, require further correction processing (PCI Geomatica, 2000). Geometric correction removes these distortions by referencing the image to its known geographic position on the ground (Lillesand and Kiefer, 1994, 528p).

Measurement techniques to correct these errors involve collecting ground control points (GCPs) evenly distributed over the image area of interest (PCI Geomatica, 2000). GCPs are located at well-defined and easy to recognize points on both the geocoded (corrected) and uncorrected images. The displacements of these GCPs between the uncorrected and georeferenced data sets are used to correct the errors. A least squares regression analysis is used to determine the coefficients for two-coordinate transformation equations, which relate the distorted image to the desired true map projection. Geometric correction is actually carried out in a two-step process: the transformation of the pixel coordiantes and data resampling.

All corrections performed utilized a second order polynomial mathematical model in computing an image warping transformation and the nearest neighbour interpolator was used for pixel value resampling. First, the second order polynomial transform is computed based on the chosen ground control points and warps the image to fit the geometric coordinates of these GCPs. Following the polynomial transform, the nearest neighbour interpolator determines the new digital number values for each image pixel from the closest pixel to the specified input coordinates without any data averaging. In

this way the original grey level values of pixels are not significantly altered, which is important if the true backscatter signals of image features are needed.

Images for this project were geometrically corrected by first correcting an optical sensor Aster (Terra satellite) image of the study site to a digital vector file obtained from the Thai Ministry of Land Development (digitized from a 1:50,000 map sheet). There are three reasons why the Aster image was needed to perform geometric correction:

1. The vector file for roads was much too detailed and inaccurate so corresponding roads could not be found on the Radarsat image. Also, the roads on the radar image do not show up well as they are all secondary and tertiary roads. The small amount of land in the imagery does not include any main highways, which would be visible.
2. The vector file for coast lines and water bodies was accurate in the study area (checked with GPS), but the coast line on the Radarsat imagery is very blurry so RMS errors in attempted corrections were very high.
3. The Aster imagery has a very distinct coast line and river edge, which enabled an accurate correction to the coast line vector file.

Once the Aster image was corrected it was used to perform an image to image correction of the May 17, 2002 Radarsat image, which was then used to correct the four remaining project images.

The geometric correction procedure successfully overlapped the five project images in preparation for further analysis. Root mean square errors for all corrections were kept under 1.6 (as seen below in Table 5), which means the corrections may be off

by as much as 1.6 pixels in each direction, or approximately 13 meters in this case (1.6 multiplied by 8 meters). The sources of error in this correction procedure may be due to the difference in resolution between the 8 meter Radarsat imagery and the 15 meter Aster imagery. However, the goal of the correction was to allow the accurate alignment of the five Radarsat images, not to obtain perfect correction to true ground coordinates.

Table 5 Geometric correction results displaying the RMS (root mean square) error

DATE (2002)	Ground Control Point (GCPs) Collection Method	Accepted GCPs	Polynomial Order	RMS (pixels)	xRMS (pixels)	yRMS (pixels)
April 8	Image to image (May 17 image master)	10	2	1.58	1.35	1.14
May 17	Vector to image (Aster image master)	15	2	1.43	1.02	1.03
May 26	Image to image (May 17 image master)	12	2	1.45	1.40	0.71
June 10	Image to image (May 17 image master)	16	2	1.03	0.64	0.43
July 6	Image to image (May 17 image master)	10	2	1.38	0.45	1.46

4.1.3 Image Subsetting

The original Radarsat images cover approximately 50 square kilometers, which is far larger than the study area. Accordingly, the image was subset to include an area that contains gear surveyed during the field study. Subsetting creates smaller file sizes and allows for faster processing time on later processing techniques. For example, the May 17 raw image is 821 megabytes in size and has pixel and line coordinates of 0,0 in the upper left and 11812, 18226 in the lower right, whereas the subset of this image is 218 megabytes in size and has the pixel and line coordinates of 0,0 and 6000, 9500 respectively.

Image subsetting was performed twice. The first subsets were created from the five 32-bit amplitude images to decrease the file sizes, enabling faster processing time and requiring less hard drive space. Table 6 displays the before and after subset file sizes and extents in pixel and line format.

Table 6 Image file sizes and extents before and after subsetting

Date (2002)	Size Before (megabytes)	Size After (megabytes)	Extent Before (pixel/line)	Extent After (pixel/line)
April 8	916	400	12338/18527	10800/9700
May 17	821	218	11812/18226	6000/9500
May26	855	217	12297/18222	5800/9800
June 10	825	232	11801/18317	6200/9800
July 6	916	426	13553/17712	11500/9700

These images were used for the speckle filtering step and then were scaled down to 8-bit files for more efficient segmentation and classification processes. The scaled images were then subset down to 1100 pixel by 1100 line files in order to speed the final processing steps and to focus on a section of the images that contained three of the main fishing and aquaculture gears covering approximately 8.8 square kilometers.

4.1.4 Speckle Filtering

Radar satellite images are formed when electromagnetic radiation is scattered from the ground and returned to the satellite antenna to be recorded. Various physical characteristics of the ground cover will modify both the amplitude (strength) and phase (distance between the scatterer and the radar sensor) of the radiation backscattered from the ground (Smith, 1996; Oliver and Quegan, 1998; Costa, 2000). The SAR image

created from this process has a level of graininess referred to as speckle, which occurs when the radiation reaches a resolution cell on the ground and the energy interacts with many point scatters within that cell (Oliver and Quegan, 1998; Rajesh *et al.*, 2001). Each energy scattering object alters the phase and amplitude of the radiation within the resolution cell, and a combination of these changes forms the backscatter value that is returned to the radar sensor as a single signal (Costa, 2000). The phase difference in these multiple scatterers is the source of the image speckle (Raney, 1998; Costa, 2000). Image pixels with a strong signal, resulting from constructive backscatter, will produce a bright pixel where the resultant digital number value is greater than the multi-scatter mean (the mean DN value of all the scatters in that resolution cell) (Frulla *et al.*, 2000; Kushwaha *et al.*, 2000). Conversely, pixels with a faded down (weak) signal will display a dark tone resulting from deconstructive backscatter effects, where the resulting digital number is less than the multiscatter mean (Frulla *et al.*, 2000; Kushwaha *et al.*, 2000). The presence of this noise-like signal reduces image interpretability considerably as fine patterns, or areas with little contrast, are radiometrically altered beyond feature recognition (Burniquel and Lopes, 1997; Rees and Satchell, 1997; Rajesh *et al.*, 2001). For this reason, image processing steps were developed to decrease the effect of speckle by averaging or smoothing the grey level pixel values in regions of intense speckle (Touzi, 1999).

Image filtering is used to sharpen or smooth the information in an image by altering the pixel values on the basis of the grey level of its surrounding pixels. Radar images require special filters called adaptive filters, which apply algorithms to smooth image speckle while maintaining high-pass features such as edges (Loos, 2001). These

filters use local statistics by taking a weighted average of pixel values, and seem to preserve both textural and radiometric information (Lopes *et al.*, 1990). The most common adaptive filters for decreasing SAR speckle include the Frost, Lee, Kuan and Gamma MAP filters (Lopes et al., 1990; Oliver and Quegan, 1997; Costa, 2000). Theoretically, adaptive filters require large window sizes to correctly estimate the local statistics (Gineste, 1999). The filter window is a square window with odd number dimensions where each pixel in the window is averaged according to its neighbours grey level values (PCI Geomatica, 2001). In practice, a small window is commonly used as larger windows encounter too many structural features, both blurring the image and making the estimate of average feature intensity too high (Gineste, 1999). The best filter for an image scene will decrease the speckle effect and enhance edges, while maintaining a close mean pixel value to the raw image and at the same time reducing the pixel standard deviation to a minimum level (Kushwaha *et al.*, 2000).

PCI's Xpace was used to test the Lee, enhanced Lee, Frost, enhanced Frost, Kuan and Gamma adaptive filters on the April 8, 2002 image to find the best filter for the study. Both 3x3 and 5x5 filter windows were tested. The best filter for this data set was determined to be the Kuan filter as demonstrated in the results section on page 64. This filter was then applied to all five of the project images.

The Kuan filter effectively changes the multiplicative noise in the data to a signal dependant additive noise to smooth the data variance, then applies the minimum mean square error (MMSE) criterion (PCI Geomatica, 2001) to maintain edges in areas where data values change greatly from one pixel to the next. This filter works with a filter

window size range of 3x3 to 11x11 pixels. The resulting grey level value for a smoothed pixel is calculated as in Equation 6 (PCI Geomatica, 2001).

New Pixel Value	R = CP*W + I* (1-W)	Equation 6

Where:

R: new pixel value
Cu: 1 / NLooks
Ci: VAR / I
W: (1-Cu/Ci) / (1+Cu)
I: Mean grey level in the filter window
CP: central pixel in the filter window
VAR: variance in the filter window
NLOOKS: number of image looks

4.1.5 Image Scaling

Linear image scaling of the grey levels was performed to reduce the images from high resolution 32-bit files to lower resolution 8-bit files (PCI Geomatica, 2001). This step was performed after the speckle filtering so as not to alter the digital number values when testing for the best adaptive filter. The linear function was chosen to equally scale data from the 32-bit input range to the 8-bit output range (PCI Geomatica, 2001). By using the mean pixel value for each image plus three standard deviations ($\mu + 3\sigma$) for the maximum input value, which allowed for the use of 99% of the original data, only 1% of the data were lost in the data compression (Costa, 2003).

4.2 Image Processing

4.2.1 Segmentation

The process of segmentation spatially subdivides an image into separate regions with similar characteristics, enabling recognition of objects of interest (Gonzalez and Wintz, 1987; Baatz and Schäpe, 2000). According to Gonzalez and Wintz (1987) there are three main concepts of image segmentation: pixel-based, edge-based and region-based. Pixel and edge-based segmentation algorithms rely on grey level discontinuity, while region-based segmentation relies on grey level similarity and uses seed points to begin region growing (Gonzalez and Wintz, 1987). Segmentation algorithms of these types use image spectral or backscatter values to produce homogenous regions within an image by use of thresholding techniques. Currently, Segl and Kaufmann (2001) discuss two categories of image segmentation techniques: region based and edge based. The region-based techniques cluster the pixels of an image according to certain criteria such as spectral homogeneity, contrast, size or texture, while the edge based methods use edge detection filters to extract the contours of an object (Segl and Kaufmann, 2001). Both of these approaches to image segmentation use unsupervised algorithms and are, again, based on the use of thresholds (Segl and Kaufmann, 2001).

Segmentation is used as a pre-classification step on SAR images to group together pixels with similar backscatter values (Oliver and Quegan, 1997; Costa, 2000), which smoothes an image much like an adaptive filter. Multiresolution segmentation is a region-merging segmentation type found in Definiens Imaging eCognition software, which focuses on segmentation and classification. This segmentation algorithm has potential for processing textured data such as SAR imagery because, as Costa (2000)

points out, the large backscatter variability created by image speckle in SAR imagery decreases the ability to segment out homogenous regions based only on backscatter, making the option of spatial consideration important. The spatial or shape characteristics within an image can be used in conjunction with the backscatter values to identify regions of homogeneity and improve object classification.

Multiresolution segmentation starts from a limited number of single pixels, which grow into regions until they reach a cut-off criterion, or a threshold value above which pixels will no longer belong to the specific region being created (Definiens Imaging, 2003). This segmentation type is therefore a local optimization clustering process that minimizes the weighted heterogeneity (Equation 7) (Definiens Imaging, 2003).

Weighted Heterogeneity	$WH = nh$	Equation 7

Where:

WH: weighted heterogeneity
n: segment size
h: arbitrary definition of heterogeneity

Two image objects are merged if the heterogeneity growth is lower than the threshold as defined by the scale parameter, whereas if the heterogeneity growth exceeds the threshold, the region growing process stops (Definiens Imaging, 2003). Multiresolution segmentation was chosen for this project to determine if segmentation improved the gear separation and to test it as a pre-classification step.

One of the main problems with traditional, bottom-up image segmentation algorithms is the large number of possibilities when dividing an image into homogenous regions (Baatz and Schäpa, 2000). A bottom-up approach to segmentation is data driven

and uses statistical methods and parameters to process an entire image into homogenous segments, or compress the data. A top-down approach is knowledge driven and the user knows what to extract from the image and develops a model to find the best methods to extract the desired segments (Baatz and Schäpe, 2000). The main difference between the two approaches is that the top-down method is a supervised segmentation and leads to local results based on the model descriptions, whereas bottom-up approaches are unsupervised and segment the entire image based on clustering statistics, making them faster and easier to implement (Baatz and Schäpe, 2000) and better for future applications in absence of top-down knowledge.

For this project, eCognition's bottum-up, region-merging multiresolution segmentation approach was tested to find the best parameters to separate the three types of fishing and aquaculture gear in the study site subset into meaningful segments. First, segmentation was applied to both the filtered and unfiltered data to evaluate the results and determine the necessity of the image filtering process. Further segmentation tests were run on the filtered images to determine the best parameter values to obtain visually acceptable image object segments for the image subset and to find the segmentation parameters that allowed the most accurate image classification. The F5, F4 and F2 incidence angle images were tested separately and together to determine if one incidence angle, or a specific combination of angles, performed better in the image segmentation trials. This was done by comparing the brightness values from each incidence angle as well as from a composite of all the angles. The brightness value is the image mean value for pixels known to contain gear signatures.

The heterogeneity criterion consists of a criterion for tone and a criterion for shape, the latter of which is broken down into subcriteria of smoothness and compactness (Definiens Imaging, 2003). The tonal or colour criterion describes the change in heterogeneity when two image objects are merged according to the weighted standard deviations (controlled by the scale parameter) (equation 8), whereas the shape criterion describes the improvement of object shape regarding compactness and smoothness respectively (equations 9 and 10) (Definiens Imaging, 2003).

Colour	$h = \Sigma\, w \cdot \sigma$	Equation 8
Compactness	$h = l / \sqrt{n}$	Equation 9
Smoothness	$h = l / b$	Equation 10

Where:
h: heterogeneity criterion
w: weights for each segmentation level
σ: standard deviation
l: object border length
$\sqrt{n}$: square root of number of pixels forming object
b: border length

In most cases it is advantageous to mix the criterion for colour (backscatter) with the criterion for shape to reduce the deviation from compact or smooth objects, especially with highly textured radar data (Definiens Imaging, 2003). The values given to colour and shape are one decimal place fractions and must add to 1. For example, colour may have the value 0.6 and shape the value 0.4. Similarly, the values for smoothness and compactness within the shape criterion must also add to 1. For this project various

combinations of weightings were tested to determine the values that would best separate the three gear types in the image subset.

The colour and shape criteria are the main determiners of the quality of segmentation an image can attain, however several other parameters may be altered at this processing stage to improve the algorithms strength (Definiens Imaging, 2003). One such parameter is image channel weighting, which can be used to include more or less information from any of the image channels available. An image channel is a location on an image file that contains one complete image scene. In this case, each of the five project images is located on one of five available channels. Channel 6 (May 17) and 8 (June 10) were given a weighting of zero and channels 7 (May 26), 9 (April 8) and 10 (July 6) were given weightings of 1. Channel 6 and 8 images did not show as much gear information, as the sea surface was rougher on these two imaging dates. Table 7 below lists the channel locations of the five Radarsat images used in this project as well as their weighting in following processing steps.

Table 7 List showing image to channel designations and image weighting for the segmentation process

Image Date	Image Channel	Image Weighting
May 17	6	0
May 26	7	1
June 10	8	0
April 8	9	1
July 6	10	1

A second parameter, the scale parameter determines the maximum allowable heterogeneity for the image objects formed (Definiens Imaging, 2003). For this project

various tests were performed to determine the best processing level for the data, as a higher value creates larger image objects. Finally, a choice can be made between a diagonal pixel neighborhood and a plane pixel neighborhood to determine if an object will be broken into two objects or considered one. The plane neighborhood only considers a pixel to be a neighbor if it is connected on one of the four planar borders, whereas the diagonal neighborhood includes all eight of a pixel's neighbors (Definiens Imaging, 2003). For this project the plane pixel neighborhood was used as the structures of interest are not too close to the image pixel scale and this process is much more time efficient than the diagonal neighborhood (Definiens Imaging, 2003).

4.2.2 Classification

The main objective of image classification is to automatically place all image pixels or objects into land cover or land use classes (Lillesand and Kiefer, 2000). The classified data can then be used to create thematic maps of the image land cover, or to produce land cover statistics on the available classes (Lillesand and Kiefer, 2000). Traditionally, image classifiers utilize the spectral or backscatter quality of an image to categorize the image pixels into homogenous classes, however with new program developments, object shape and other spatial characteristics can be used to classify image data.

There are two main types of image classifiers: supervised and unsupervised. In supervised classification the user controls the classifier by providing numerical descriptor samples of the various land cover types in an image scene. These sample sites are known as *training sites* and train the algorithm to recognize numerical patterns for each class present in an image. The algorithm then goes through the image and classifies each pixel

or segment based on these descriptors. In this case, the user has a-priori knowledge of the study area in order to select representative training sites and determines the level or scale of classification that results. Classes will only be created if the user determines them to be present in the study area.

In the case of unsupervised classifiers, the user may not have any knowledge of the land cover in the image scene. Unsupervised classifiers do not use training data to classify image data; instead they use clustering algorithms that aggregate pixels into statistically similar groups. The basic premise behind unsupervised classifiers is that the numerical values of a specific cover type will be close together in measurement space, while numerical values from different classes will be well separated (Lillesand and Kiefer, 2000). The algorithm is run on an image with much iteration and a given number of classes to develop in order to determine the location of class centers. Once these centers are determined, each pixel or segment will be classified according to its distance from, or location in relation to, the class centers, depending on the algorithm. Unlike the supervised classification where the user predetermines the classes, the user must name the classes created by an unsupervised classification, a step that requires reference data for the study area.

eCognition is a knowledge-based, object-oriented segmentation and classification program that considers an object's size and scale as well as backscatter and shape characteristics (Baatz and Schäpe, 2000). The large amount of knowledge that the user can supply allows for more detailed classification analysis. eCognition uses a fuzzy rule base for classification where one or more conditions are combined by operators to determine the membership of an image object to a specific class (Definiens Imaging,

2003). Membership functions allow the inclusion of knowledge that the user may have on a particular class that will help to separate this class from any other image feature (Definiens Imaging, 2003). For example, the user may know that the mean digital number value for a particular class is very high compared to other classes, so can formulate this information into a membership function and automatically separate this class from all others.

eCognition only offers a supervised classification so the user must be familiar with the study area in order to collect acceptable training sites or class samples. There are two options within the supervised classification: nearest neighbor, which automatically generates multidimensional membership functions based on the chosen samples, and membership function dialog, which creates one-dimensional membership classes with a graphical interface (Definiens Imaging, 2003). For this project the nearest neighbor classifier was used because several object features were used to describe the classes and according to Definiens Imaging (2003), the nearest neighbor classifier evaluates the correlation between object features better than the membership function classifier.

Initially, a class hierarchy was created with four classes: water, oyster, mussel and fishgear. Within each class the user can choose any number of object feature descriptors from a detailed list to help separate the objects into their representative classes. For this trial the mean and standard deviation values were chosen to describe the image objects for each class. The minimum and maximum of these values were determined and entered into the membership function dialog box using an about range function. The function slope describes the calculation of the membership value for an expression for a particular

class and determines a segment's inclusion or exclusion from that class, as seen below in Figure 21. The x-axis is the value range that an image object must fit into to be considered part of that class. For example, the full range membership function will include all objects whose values are between the lower and upper bounds of the x-axis, whereas the about range function will gradually exclude image objects at either end of the graph with values that fall in the thirteen percent tails of the full range.

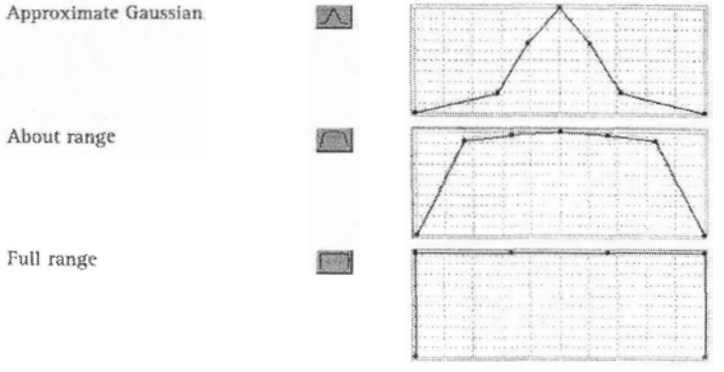

Figure 21 Membership function types (Gaussian, about range and full range) (modified from eCognition manual, 2003)

The mean and standard deviation were chosen as object descriptors because these values in the sample data appeared to support a level of signature separation as seen in Table 8. Five representative sample objects of each gear type were selected from the image to begin testing the algorithms ability to separate the gear. The training samples were chosen based on knowledge from field sampling and attempted to cover the range of each gear type's backscatter values. Definiens Imaging (2003) suggests starting with a small number of samples, running the classification, then adding more samples to improve the classification results by choosing miss-classed objects as new sample objects.

Table 8 Mean, standard deviation and colour of 12 samples for the four-class test on the five Radarsat images (0-255 DN scale)

		08-April-02		17-May-02		26-May-02		10-June-02		06-July-02	
Classes	**Colour**	**Mean**	***St.Dev.***	**Mean**	***St.Dev.***	**Mean**	***St.Dev.***	**Mean**	***St.Dev.***	**Mean**	***St.Dev.***
Water	Blue	88.6	*10.64*	99.8	*10.52*	96.3	*6.35*	125.4	*7.49*	86.2	*10.65*
Oyster	Orange	248.5	*4.40*	246.1	*4.77*	245.7	*5.48*	243.8	*6.50*	242.4	*9.47*
Mussel	Green	216.6	*26.31*	187.9	*27.23*	225.2	*18.91*	182.1	*19.19*	201.7	*34.60*
Fishgear	Yellow	177.0	*47.45*	182.2	*39.78*	201.4	*39.32*	165.2	*31.40*	176.0	*48.17*

When running the classifier the function slope parameter is given a value between 0 and 1, depending on whether the user wishes to decrease or increase the distance an object may have from the nearest sample while still being classified (Definiens Imaging, 2003). A higher function slope will classify more image objects, but results in a less stable classification than a lower function slope (Definiens Imaging, 2003). A function slope of 0.5 was used for this classification attempt as trials with a lower function slope lead to many unclassed and miss-classed objects.

Once the object descriptors and the slope function had been set, the classification was run. During the process, each class description in the class hierarchy is applied to each image object of the chosen segmentation level (Definiens Imaging, 2003). An image object is then assigned to the class whose statistical evaluation results in the highest membership value and if the image object value is lower than the defined minimum membership value, then that object will remain unclassified (Definiens Imaging, 2003). The classification run with the above mentioned parameters showed poor results so attempts were made to first improve the original segmentation image by going to a higher level of segmentation, which results in larger image objects. Shape

descriptors such as main direction, rectangular fit, asymmetry and length/width ratio were also added into the class descriptor list with their respective minimum and maximum values and about range and full range membership functions to help improve class separation. The results from these changes, although improved, still reported poor class separability.

In response to the poor separation results a new set of classes was developed by breaking the previous four classes into nine, more specific classes, as shown below in Table 9. The object feature descriptors chosen to separate the classes were retested for the new class set and the features that reduced the digital number overlap best were used as descriptors for further classifications.

Table 9 Mean, standard deviation and colour of samples for the nine-class test on the five Radarsat images

		08-April-02		17-May-02		26-May-02		10-June-02		06-July-02	
Classes	**Colour**	**Mean**	***St.Dev***	**Mean**	***St.Dev***	**Mean**	***St.Dev***	**Mean**	***St.Dev***	**Mean**	***St.Dev***
Water Dark	Dark Blue	84.1	*2.55*	97.3	*5.44*	97.8	*6.26*	120.9	*8.08*	84.9	*1.94*
Water Medium	Medium Blue	94.6	*2.81*	106.2	*9.48*	100.8	*6.86*	132.5	*11.30*	95.0	*2.84*
Water Light	Light Blue	119.1	*10.63*	117.3	*15.02*	115.3	*11.12*	146.3	*13.06*	121.3	*11.75*
Oyster Large	Orange	227.2	*14.73*	233.6	*13.81*	228.1	*17.81*	229.3	*14.37*	224.5	*16.09*
Oyster Small	Cream	224.9	*15.65*	229.3	*12.42*	226.9	*17.04*	221.4	*18.31*	220.8	*16.11*
Fishgear Codend	Yellow	230.9	*17.24*	211.2	*24.75*	230.2	*19.73*	186.5	*22.07*	227.2	*19.01*
Fishgear Guides	Brown	179.7	*29.05*	160.1	*30.61*	167.5	*39.49*	137.1	*10.83*	171.4	*34.24*
Mussel Dark	Dark Green	143.9	*17.57*	155.5	*16.63*	171.5	*28.69*	158.2	*17.02*	135.7	*18.95*
Mussel Light	Light Green	224.5	*16.52*	210.8	*18.25*	219.3	*17.53*	182.6	*30.02*	218.1	*19.35*

The low class separation is related to the similarities among the three gear types. The stationary fishing gear is composed of two main parts structurally: the codend and

the leaders. The codend has the same backscatter value as the oyster gear and are similar in shape to the mussel gear segments, while the leaders have the same backscatter values as the mussel gear as well as a similar shape to the smaller oyster gears. These backscatter and shape overlaps decrease the algorithms ability to separate the different gears in the study area.

To attempt separation of the three water class objects the mean descriptor was used with a full range membership function, as the water objects had distinct differences in digital number value from each other and from the gear image objects. The full range membership function was used to determine distinct class cut-off points. The oyster gears displayed in the image had two distinct sizes and very similar digital number values to each other and to the fishing gear codend objects. Descriptors were tested to create two oyster classes and to attempt to separate the oyster from the fishing gear codend. The mean descriptor was used with an about range function as well as the length and width descriptors from the shape component, which were found to show slight differences between the gear size classes. The about range membership function cuts off approximately five percent of the information from either end of the function slope, narrowing the extremities of the range. The length and width descriptors were used with a full range membership function to provide a distinct cut-off point between the two oyster classes according to size. Further, to separate the fishing gear codend and guides from each other and from other image objects, the mean difference to neighbors and rectangular fit descriptors were used with about range and full range membership functions respectively. The codend and guides have very different shape as well as backscatter values from one another, but are each similar to other gears in the scene. The

mussel gear seemed to appear both light and dark in the image and have a different shape than many of the other image objects so the mean descriptor was used with a full range membership function as well as the asymmetry descriptor, also with a full range function. Creating more classes (nine) with narrower ranges lessened the class overlap and improved classification results. Summaries of the various classification tests run with both four and nine classes are shown on the following pages in Table 10 and Table 11.

Table 10 Classification tests with 4 classes

	Object Descriptors			
Classes	**Spectral**	**Spatial**	**Membership Function (range)**	**Function Slope**
Water	mean / st.dev.	-	about	0.5
Oyster	mean / st.dev.		about	
Fish Gear	mean / st.dev.		about	
Mussel	mean / st.dev.		about	
Water	mean / st.dev.	rectangular fit	about / full	0.5
Oyster	mean / st.dev.	rectangular fit	about / full	
Fish Gear	mean / st.dev.	rectangular fit	about / full	
Mussel	mean / st.dev.	rectangular fit	about / full	
Water	mean / st.dev.	rectangular fit	about / full	0.5
Oyster	mean / st.dev.	length/width ratio	about / full	
Fish Gear	mean / st.dev.	rectangular fit	about / full	
Mussel	mean / st.dev.	length/width ratio	about / full	
Water	mean / st.dev.	main dir. / rect. fit	about / about	0.5
Oyster	mean / st.dev.	length/width ratio	about / about	
Fish Gear	mean / st.dev.	main dir. / rect. fit	about / about	
Mussel	mean / st.dev.	asymmetry	about / about	
Water	mean / st.dev.	main dir. / rect. fit	about / full	0.5
Oyster	mean / st.dev.	main dir. / rect. fit	about / full	
Fish Gear	mean / st.dev.	asymmetry	about / about	
Mussel	mean / st.dev.	main dir. / rect. fit	about / full	
Water	mean diff. to neigh.	main dir. / rect. fit	about / full	0.5
Oyster	mean diff. to neigh.	main dir. / rect. fit	about / full	
Fish Gear	mean diff. to neigh.	main dir. / rect. fit	about / full	
Mussel	mean diff. to neigh.	asymmetry	about / about	
Water	mean diff. to neigh.	rectangular fit	about / full	0.5
Oyster	mean / st.dev.	main dir. / rect. fit	about / full	
Fish Gear	mean / st.dev.	main dir. / rect. fit	about / full	
Mussel	mean / st.dev.	main dir. / rect. fit	about / full	
Water	mean diff. to neigh.	rectangular fit	about / full	0.6
Oyster	mean / st.dev.	main dir. / rect. fit	about / full	
Fish Gear	mean / st.dev.	main dir. / rect. fit	about / full	
Mussel	mean / st.dev.	main dir. / rect. fit	about / full	
Water	mean diff. to neigh.	rectangular fit	about / full	0.7
Oyster	mean / st.dev.	main dir. / rect. fit	about / full	
Fish Gear	mean / st.dev.	main dir. / rect. fit	about / full	
Mussel	mean / st.dev.	main dir. / rect. fit	about / full	

Table 11 Classification tests with 9 classes

	Object Descriptors			
Classes	**Spectral**	**Spatial**	**Membership Function (range)**	**Function Slope**
Water (3classes) Oyster (2 classes) Fish gear (2 classes) Mussel (2 classes)	Mean diff. to neigh. mean / st. dev. mean / st. dev. mean / st. dev.	length/width ratio main direction length/width ratio asymmetry	about / full about / full about / full full / full	0.5
Water (3classes) Oyster (2 classes) Fish gear (2 classes) Mussel (2 classes)	Mean diff. to neigh. mean mean mean	length/width ratio main direction rectangular fit asymmetry	about / about about / about about / about full / about	0.5
Water (3classes) Oyster (2 classes) Fish gear (2 classes) Mussel (2 classes)	Mean diff. to neigh. mean mean mean	- main dir. / rect. fit rectangular fit asymmetry	about about / full /about about / full full / full	0.5
Water (3classes) Oyster (2 classes) Fish gear (2 classes) Mussel (2 classes)	Mean diff. to neigh. mean mean diff. to neigh. mean	- rectangular fit rectangular fit asymmetry	about about / full about / full full / full	0.5
Water (3classes) Oyster (2 classes) Fish gear (2 classes) Mussel (2 classes)	mean mean mean mean	- main direction rectangular fit asymmetry	about about / full about / full full / full	0.5
Water (3classes) Oyster (2 classes) Fish gear (2 classes) Mussel (2 classes)	mean mean mean diff. to neigh. mean	- length/width ratio rectangular fit asymmetry	about about / full about / full full / full	0.5
Water (3classes) Oyster (2 classes) Fish gear (2 classes) Mussel (2 classes)	mean mean mean diff. to neigh. mean	- length/width ratio rectangular fit asymmetry	about about / full about / full full / full	0.6
Water (3classes) Oyster (2 classes) Fish gear (2 classes) Mussel (2 classes)	mean mean mean diff. to neigh. mean	- length/width ratio rectangular fit asymmetry	about about / full about / full full / full	0.7
Water (3classes) Oyster (2 classes) Fish gear (2 classes) Mussel (2 classes)	mean mean mean diff. to neigh. mean	- length/width ratio rectangular fit asymmetry	about about / full about / full full / full	0.6

Some abbreviations used in the tables for the object descriptors are defined below:

mean diff. to neigh. = mean difference to neighbors
st. dev. = standard deviation
main dir. = main direction
rect. fit = rectangular fit

Table 10 has only four classes as written, whereas the classification descriptions from Table 11 are based on nine-class processes. The three water classes refer to dark, medium and light water segments; the oyster classes are large and small segments of this gear type; the fish gear class is divided into codend and guide classes; and the mussel classes are dark and light segments.

As mentioned on page 53, the function slope is a value between 0 and 1 that determines the distance an object must be from a sample in order to be classified. In each case the final table entry portrays the best classification results as discussed in the following chapter.

4.3 Summary

This chapter defined and described the project's methodology that was performed in an attempt to separate the three fishing and aquaculture gear types in the subset Radarsat-1 scene. The first steps, radiometric and geometric corrections were followed by image subsetting, to get the image to an acceptable size for further processing. At this stage speckle filtering was tested to determine the best adaptive filter to clarify the image speckle problem. Following this, the image was scaled down to an 8-bit image for further processing. Image segmentation and supervised classification techniques were the final processes used to attempt gear separation. The following chapter presents and discusses the project results and presents an accuracy assessment.

Chapter 5

5.0 Results and Discussion

This chapter presents and discusses the results of the data analysis and assesses the accuracy of the classifications obtained. Image pre-processing and processing steps mentioned in the methodology chapter, as well as other related issues, are also addressed.

5.1 Image Analysis

Before any pre-processing steps were begun an analysis of the raw imagery determined that the fishing and aquaculture gears were detectable on a full resolution view of the raw 16-bit data. Definite structures of the gears were not apparent at this stage; however, bright pixels appeared in the areas where gears had been found in the field study. Also, the shallower angled images (F4 and F5) appeared to provide more gear information as the greater incidence angle allowed the gears to act as strong corner reflectors.

5.2 Radiometric Correction

Each of the 16-bit unsigned intensity Radarsat images was radiometrically corrected to 32-bit real amplitude images. The corrected multi-temporal images have comparable radar backscatter values and display these values in a positive optimized range. An example from the May 17 image, shown in Figure 22 below, portrays how the DN values change after the SARSIGM process is run. The first display shows digital number values for pixels from the original 16-bit intensity satellite image, whereas the lower display gives digital number values for the calibrated 32-bit amplitude image.

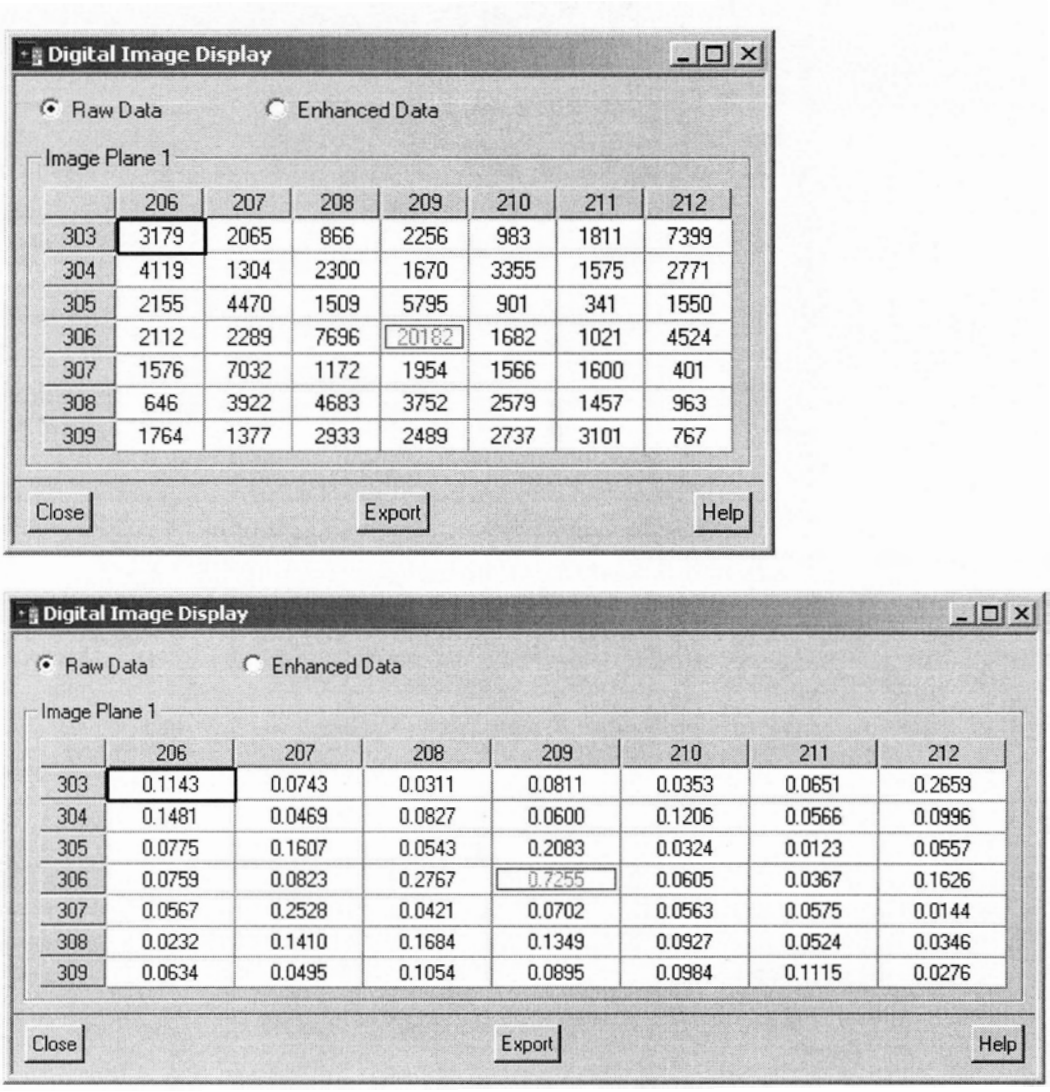

Figure 22 Digital number values for the same pixels from the 16-bit intensity image (above) and the 32-bit amplitude image (below), where each cell corresponds to a pixel in the image

The new amplitude values are comparatively small because the amplitude is the square root of the intensity value and the range of the new 32-bit file (-10 exp38 to + 10 exp38) is much greater than that of a 16-bit file (0 – 65,535) (Filion, 2003). The pixel value displays in Figure 22 correspond to the image below in Figure 23. The central cell in the display above, surrounded by a grey box, relates to the pixel containing the crosshair in the image below, while surrounding cells correspond to the respective surrounding image pixels.

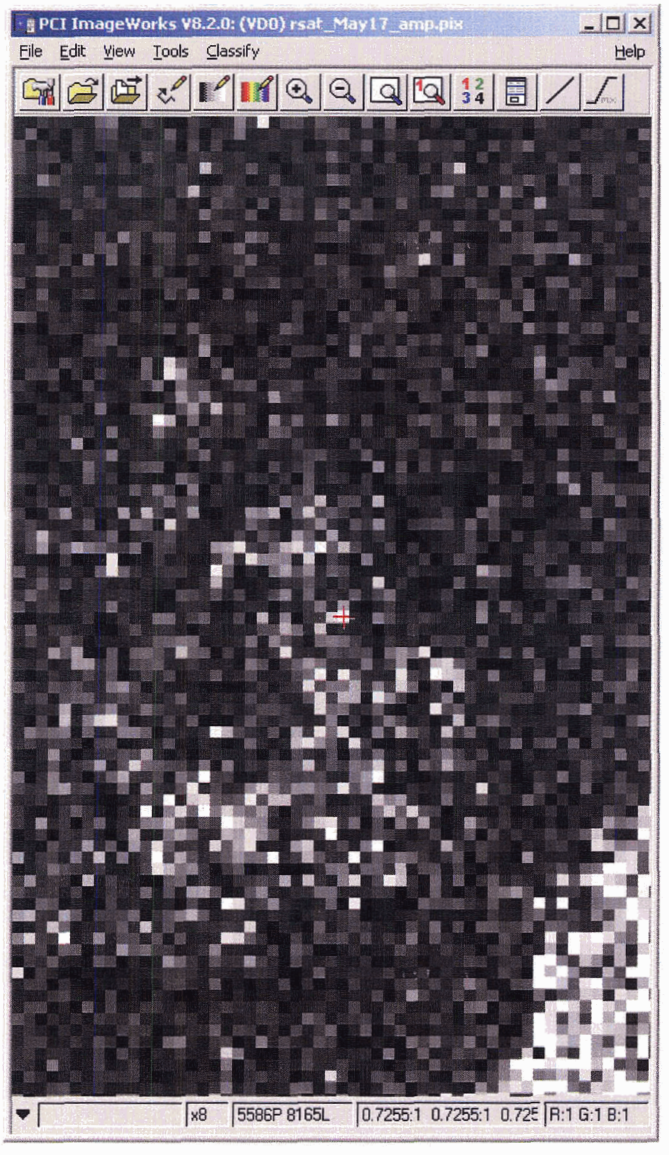

Figure 23 Amplitude image zoom on aquaculture gear in water. The red crosshair represents the pixel that corresponds to the above DN value in the central box of the digital image displays of Figure 23

The displays from Figure 22 give the values for 3 pixels in all directions of the central cell, which correspond to the 3 pixels in any direction from the bright pixel with the red crosshair in Figure 23. The display cell value of 20182 is the intensity value from the original data, which through the calibration process becomes 0.7255 as a 32-bit amplitude value. The histogram in Figure 24, from the zoomed image of Figure 23, shows that the

majority of the amplitude digital number values are below a value of 0.65, with a minimum value of 0.0001 and a maximum value of 2.4070. In the image itself most of the pixels represent water, which has a low backscatter value resulting from specular reflection off the water surface. The histogram suggests that water pixels have an amplitude value below 0.65 and that fishing and aquaculture gear values will be between 0.65 and 2.4, with the brightest pixels of the image near 2.4.

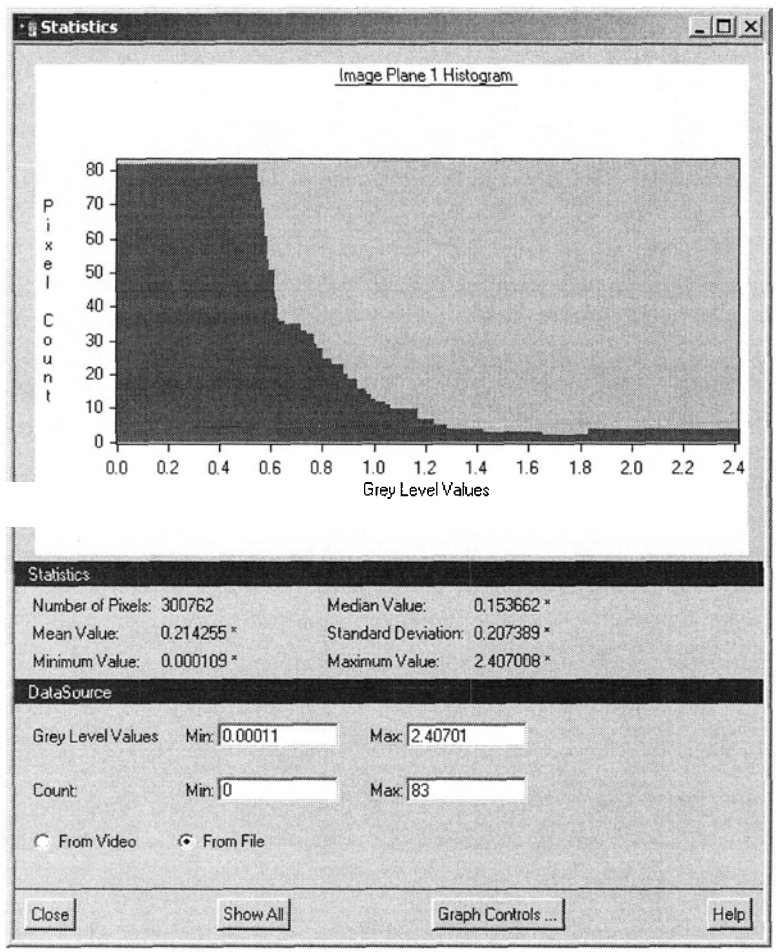

Figure 24 Histogram of the 32-bit amplitude image showing distribution of pixel DN values

5.3 Speckle Filtering

Adaptive filtering was applied to the 32-bit imagery in order to reduce the speckle effect caused by the phase difference from multiple scatterers in a resolution cell, thereby smoothing the image. Six filters were tested to determine the best filter for the particular data: Frost, Enhanced Frost, Lee, Enhanced Lee, Kuan and Gamma. The two best filters were then tested with both a 3x3 and 5x5 window to determine which would be used for the project. As mentioned earlier, the best filter for the imagery will decrease the speckle effect and enhance edges, while maintaining mean pixel values close to the raw data and reducing the pixel standard deviation to a minimum level. Table 12 below displays the mean, standard deviation and coefficient of variation values for each of the filters tested on the April 8, 2002 image.

Table 12 Size, mean, standard deviation and coefficient of variation for the six adaptive filters tested and the raw April 8 image

Filter	Filter Window Size	Mean (x)	Standard Deviation (s)	Coefficient of Variation (cv)
Raw Image	--	0.102	0.072	0.706
Lee	3x3	0.102	0.072	0.706
Frost	3x3	0.102	0.057	0.559
Kuan	3x3	0.102	0.056	0.549
Gamma	3x3	0.109	0.060	0.550
Enhanced Lee	3x3	0.109	0.060	0.550
Enhanced Frost	3x3	0.110	0.060	0.545
Kuan	5x5	0.102	0.048	0.471
Frost	5x5	0.102	0.049	0.480

The raw image from April 8 has a mean DN value of 0.102 with a standard deviation of 0.072, which standardizes to a coefficient of variation of 0.706. All six of the above filters were applied to this raw image with a 3x3 filter window to determine how they altered the DN values. The 3x3 window translates to a 576 m^2 area on the water. From the results, the Kuan and Frost filters both kept the mean DN value the same as the raw image and at the same time lowered the s and cv. However, the Kuan filter lowered these values more than the Frost filter. The Lee filter also kept the same mean DN value, but did not lower the s and cv, while the Gamma and both of the enhanced filters increased the mean DN value.

The Kuan and Frost filters were then tested with a 5x5 window to determine the best filter window size for the data. Both of these filters kept the mean pixel DN value stable and further lowered the standard deviation, which would suggest the 5x5 window lessens the speckle effect more than the 3x3 window. However, visually, some of the features appeared over-smoothed so the Kuan 3x3 filter was chosen to apply to all five images. Filtering was performed prior to the image scaling, as scaling alters the raw DN values.

5.4 Image Scaling

A scaling of the grey level values reduced the images from 32-bit files to lower resolution 8-bit files, which also decreased the file size significantly. The scaled 8-bit data have DN values ranging from 0 to 255. The input minimum and maximum values were calculated using the DN mean minus three times the standard deviation and the DN mean plus three times the standard deviation respectively. Table 13 displays these values for each of the five images. The input minimums are always zero as the $\mu - 3\sigma$

calculation yields negative numbers, which are not acceptable in an amplitude image. The output minimum and maximum values used to perform the scaling process are 0 and 255 for an 8-bit image.

Table 13 Mean, standard deviation, scale factor, input min and max values for image scaling

Image	Mean (μ)	Standard Deviation (σ)	Scale Factor (3σ)	Input Min ($\mu - 3\sigma$)	Input Max ($\mu + 3\sigma$)
April 8	0.102	0.056	0.168	0	0.270
May 17	0.060	0.034	0.102	0	0.162
May 26	0.064	0.038	0.114	0	0.178
June 10	0.059	0.027	0.081	0	0.140
July 6	0.102	0.057	0.171	0	0.273

After scaling the digital number values increased from a range of 0 to approximately 2.4 to a range from 0 to 255. For example, in Figure 25 the first digital image display shows the pixel values for an area in the 32-bit May 17 image and the second display shows the values for the same pixels after scaling to 8-bits. Table 14 below displays the calibration statistics for the five Radarsat images.

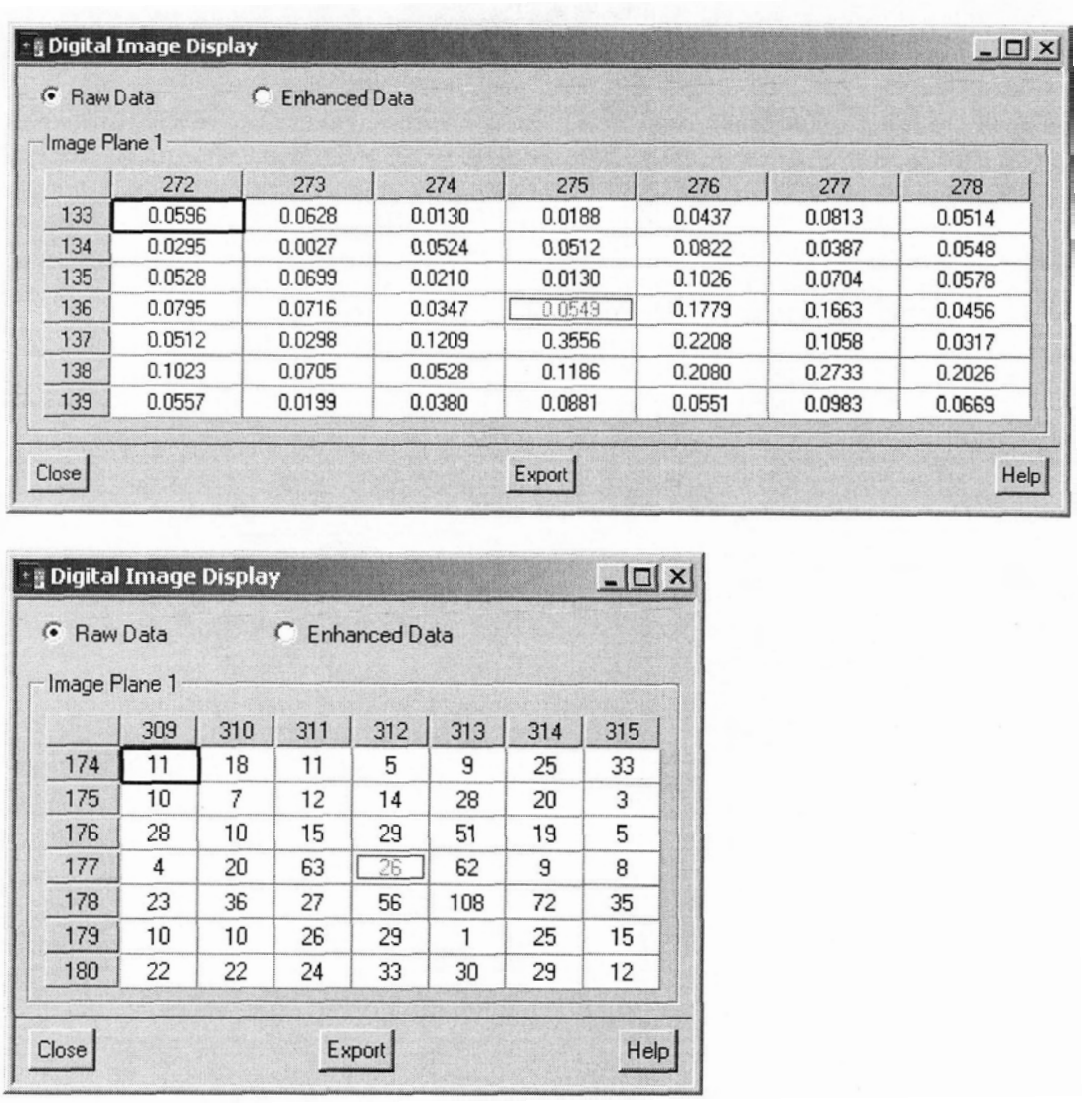

Figure 25 DN values for the same pixels from the 32-bit image (above) and the 8-bit scaled image (below), where each cell corresponds to a pixel in the image

Table 14 DN statistics for the original 16-bit and 8-bit calibrated and scaled Radarsat-1 images

	April 8		May 17		May 26		June 10		July 6	
Statistic	Orig.	Calib.	Orig.	Calib.	Orig.	Calib.	Orig.	Calib	Orig.	Calib.
Mean	4899	137.32	5983	139.99	5481	139.79	6076	154.97	4445	137.41
St. Dev.	5584	61.40	5787	62.81	6333	62.82	5938	55.40	5382	61.42
Variance	$3x10^7$	3770	$3x10^7$	3945	$4x10^7$	3947	$3x10^7$	3069	$2x10^7$	3772

5.5 Segmentation

A number of segmentation tests were applied to both the unfiltered 32-bit and filtered 8-bit data to attempt separation of the three gear types found in the image subset (oyster, mussel and stationary fishing gear) and determine the necessity of the filtering process prior to segmentation. Results show that the filtering process greatly improves the ability of the software to separate the data into meaningful segments. Figure 26 displays the unfiltered segmentation trial that produced the best segmentation results, while Figure 27 shows the much more meaningful segments from the same image after filtering.

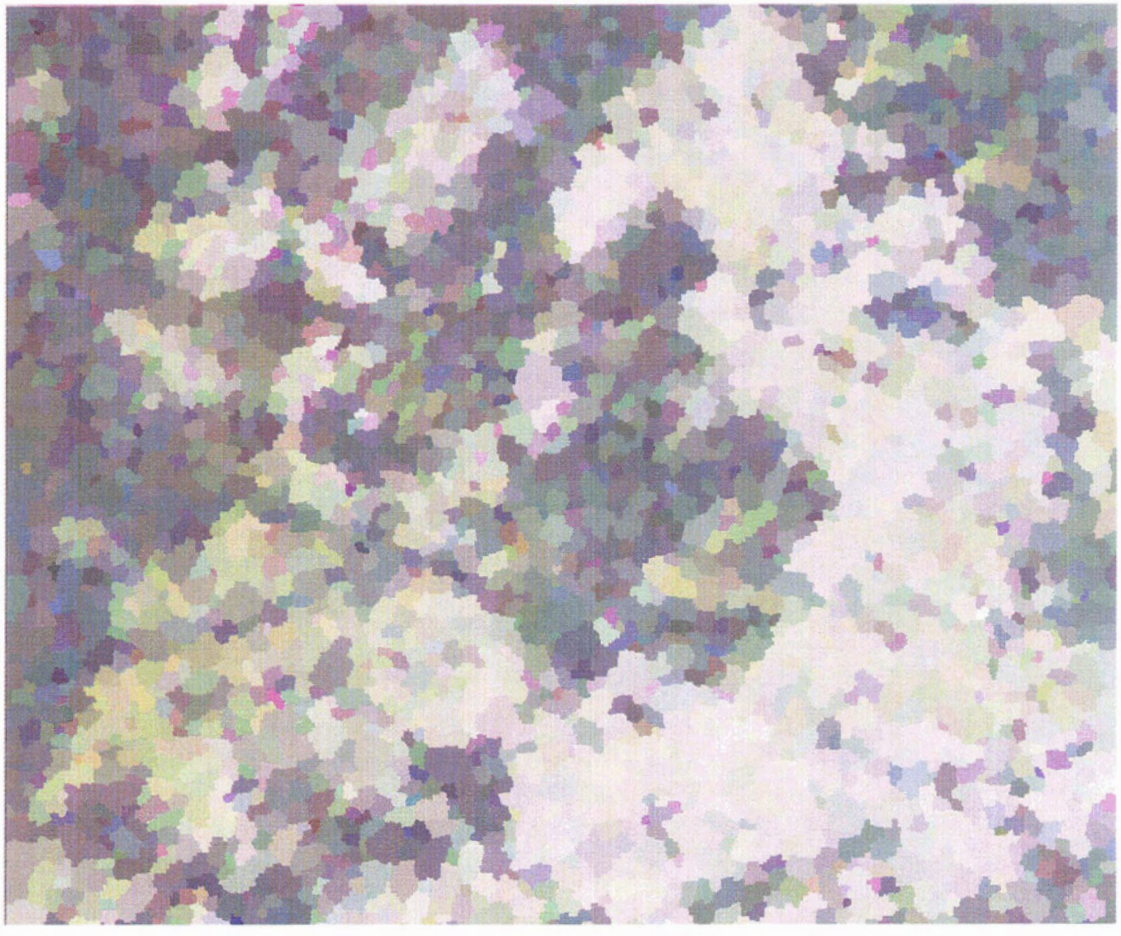

Figure 26 Segmentation of the unfiltered image subset (1:60,000)

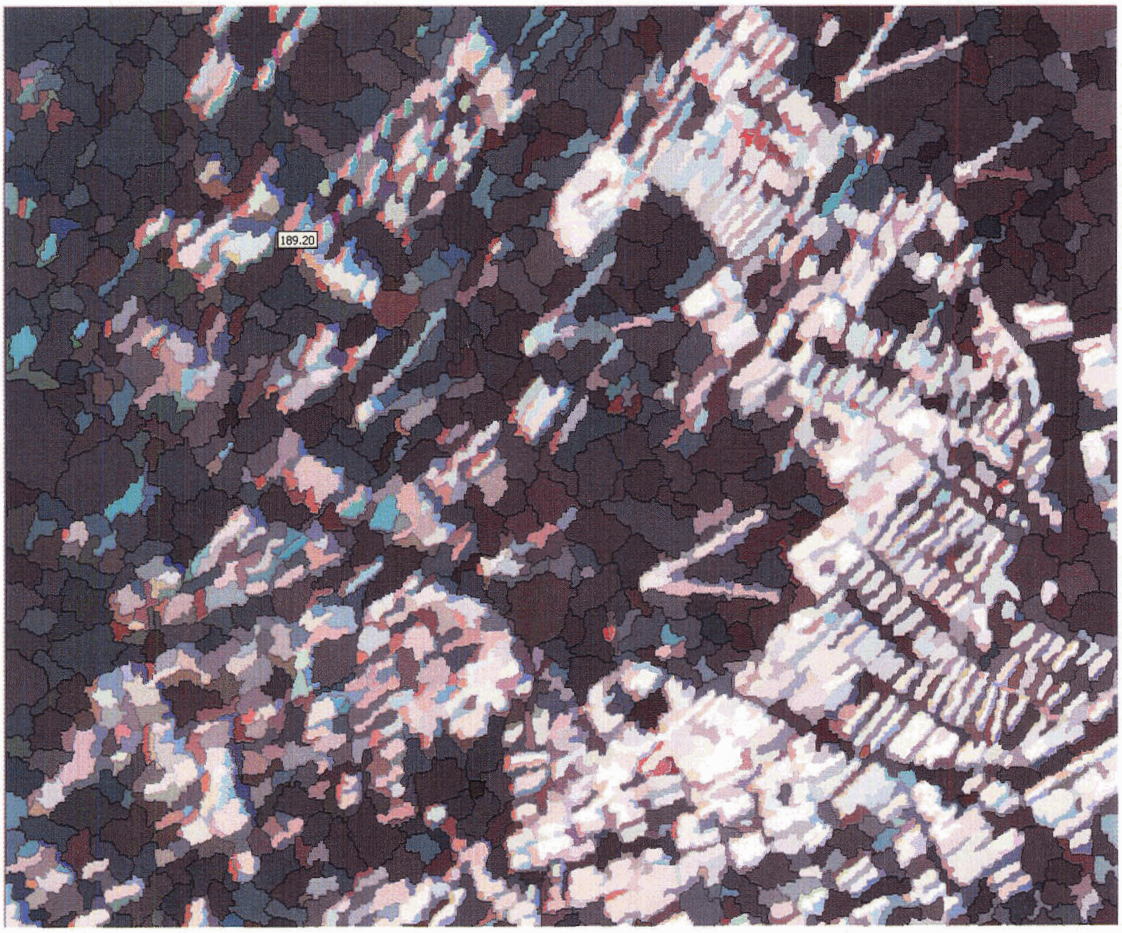

Figure 27 Segmentation of the filtered image subset (1:60,000)

The filtered image is much easier to interpret and shows the distinction between the dark water segments and the lighter gear segments clearly. Looking at the v-shaped stationary fishing gear in the center and top right of the above images it is clear that the filtering process is a necessary step when segmenting radar data. Both images were created with the following heterogeneity criterion:

Colour ⇒ 0.4
Shape ⇒ 0.6

Smoothness ⇒ 0.6
Compactness ⇒ 0.4

A range of values were tested for the heterogeneity criterion, however, making the shape criterion a bit higher than the colour criterion, as seen above, created larger segments, which increased the visual separation of the gear.

Next, tests were run to determine if one incidence angle performed better in the segmentation trials in terms of gear separation. Results showed that both visually and numerically the combination of all available incidence angles together increased the separation between the three gear types. Table 15 displays the mean brightness values for each gear type, at each incidence angle.

Table 15 Mean brightness values for mussel, oyster and fishing gear (codend and leader) segments on F5, F4 and combination incidence angle imagery, the single F2 image is not averaged

Incidence Angles	Mean Segment Brightness Values (except F2)			
	Mussel	Oyster	Codend	Leaders
F5 (2 images)	182.50	248.69	240.40	183.15
F4 (2 images)	178.59	249.03	241.56	180.39
F2 (1 image)	166.76	247.02	229.06	171.29
All Angles (5 images)	175.95	248.25	237.01	178.27

The F4 and F5 images produced very similar brightness values for all the gears, and as can be seen in Table 15, the mussel gear and fishing gear leaders have brightness values that are too similar to one another to easily differentiate, as do the oyster gear and the fishing gear codends. However, the F2 image brightness values have a more significant separation between the gear types. For example, the mussel gear has a brightness value of 166.76, whereas the fishing gear leaders have a value of 171.29. Similarly, the oyster gear has a value of 247.02, while the fishing gear codend has a brightness value of 229.06. The combination image with all available angles also shows

more significant differentiation between the gear types as it has characteristics of all the image incidence angles.

For further processing I chose to use a three image combination of the April 8 F5 image, the May 26 F5 image and the July 6 F2 image. With these images both steep and shallow angle data is represented and the June 10 F4 image, which was acquired on a wavy day and had some of the stationary fishing gears visible in both the May and July images not present, was able to be left out of further analysis. The May 17 F4 image was left out of the final analysis as it was not as clear an image as the others and had a greater amount of speckle effect, also resulting from rougher sea conditions during imaging.

After determining the best imagery to continue analysis with, further segmentation tests were run to find the best level of segmentation for gear separation and to use in the classification process. Figure 28 displays the chosen segmentation level used to continue the project. The image was created using the following heterogeneity and scale parameters as defined on pages 47 and 48:

Colour ⇒ 0.4
Shape ⇒ 0.6

Smoothness ⇒ 0.6
Compactness ⇒ 0.4

A scale parameter of 30 was used in the first level of image segmentation, which was followed by two subsequent segmentations using the same heterogeneity parameters and a scale parameter of 40 and 50 respectively. These steps created an image with relatively large, meaningful segments, which helped to visually differentiate the types of fishing and aquaculture gears in the study subset. For this reason, the image in Figure 28 was chosen to continue the process of segment classification.

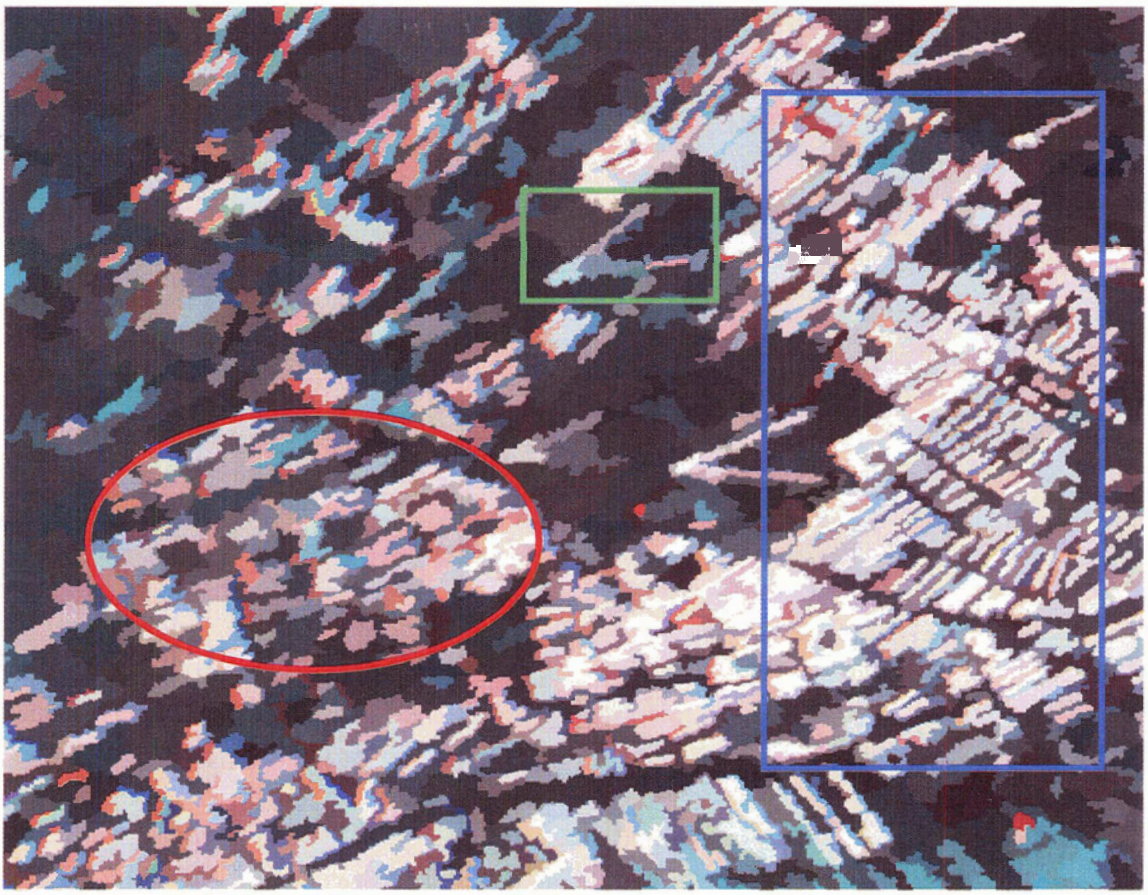

Figure 28 Best image segmentation level for visual gear separation (1:60,000)

The oyster gear, found in the blue rectangle on right hand side of the image, has a high brightness level and the segments are relatively regular shaped rectangles, whereas the mussel gear in the red oval are fairly irregular shaped and most of the segments have a darker brightness level. These two gear segments separate fairly well in terms of both shape and colour, however, the stationary fishing gear trap (v-shaped structures in green box) codends are very similar to the mussel gear and the fishing gear leaders are very similar to the oyster segments in both shape and colour. These latter gear sets are both visually and numerically difficult to separate. Figure 29 below displays the problems with the numeric separation of the gears. The mussel and fish gear overlap (d) as well as the oyster and fishgear overlap (e) can be detected in the graphs below.

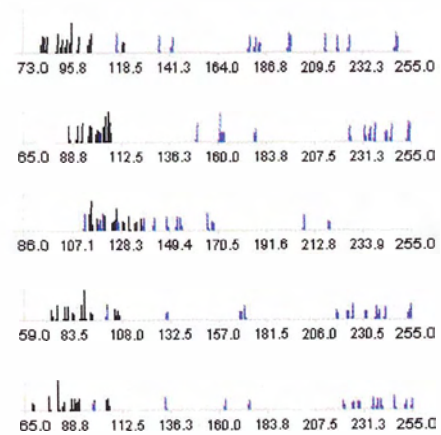

a) water (black) and fish gear

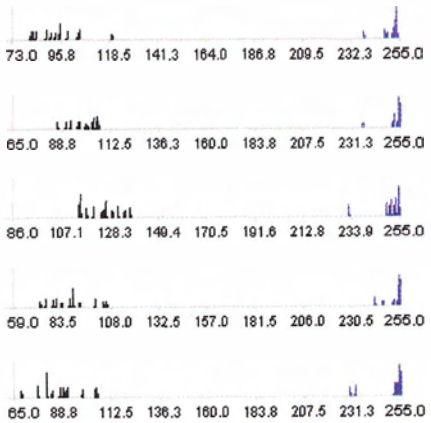

b) water (black) and oyster

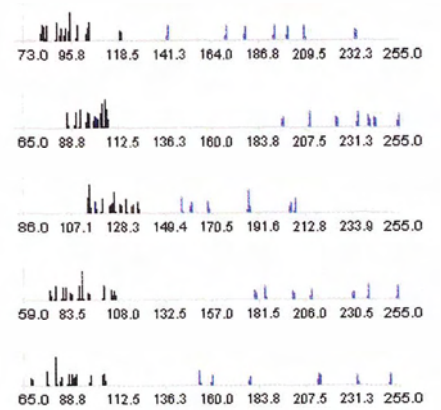

c) water (black) and mussel

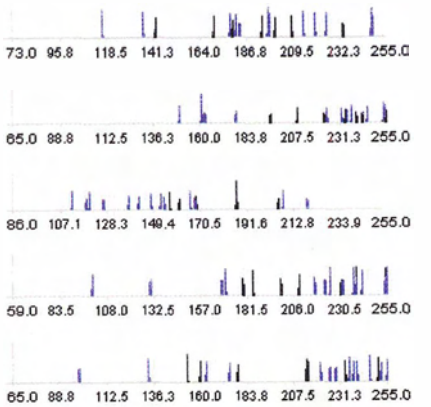

d) mussel (black) and fish gear

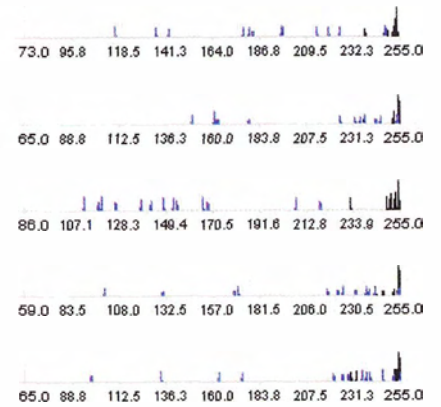

e) oyster (black) and fish gear

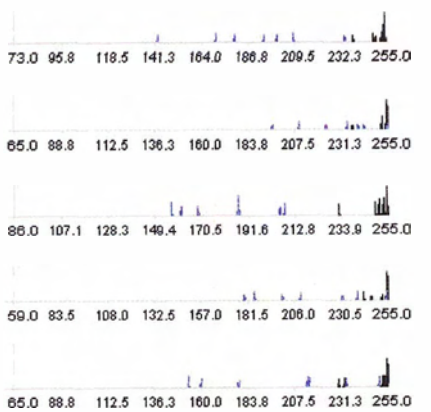

f) oyster (black) and mussel

Figure 29 Numeric separation of the class training samples for the four-class test

5.6 Classification

Various supervised classification tests were run on the segmented image from Figure 28 to determine if this process could further separate the three fishing and aquaculture gear types. Classification results from the four-class test were poor because the gear signatures digital number values had too significant of overlap, as seen in Table 16.

Table 16 Mean, standard deviation and colour of the four classes from the classification results

		08-April-02		17-May-02		26-May-02		10-June-02		06-July-02	
Classes	**Colour**	**Mean**	***Std.Dev***	**Mean**	***Std.Dev***	**Mean**	***Std.Dev***	**Mean**	***Std.Dev***	**Mean**	***Std.Dev***
Water	Blue	116.8	*14.63*	119.2	*12.59*	125.2	*14.81*	141.0	*13.76*	118.8	*14.58*
Oyster	Orange	210.3	*14.75*	215.6	*14.96*	220.1	*12.48*	199.4	*21.95*	197.2	*19.22*
Mussel	Green	192.4	*31.19*	172.6	*29.76*	177.4	*41.96*	185.8	*34.60*	186.2	*33.56*
Fishgear	Yellow	174.4	*32.20*	166.1	*28.72*	185.6	*40.33*	159.7	*21.99*	132.6	*36.26*

From the April 8 image the oyster gear has a minimum value of 196 and a maximum of 224, the mussel gear has a minimum value of 161 and a maximum of 223 and the fishing gear has a minimum of 142 and a maximum value of 206. These numbers show that most of the segments have considerable overlap in brightness values, which lead to low classification accuracy in numerous tests. Water is the only class that can clearly be separated from the others with a minimum value of 102 and a maximum of 131. Figure 30 displays the results from the initial classification using four-classes. As can be seen, many of the segments, especially gear segments, were unclassed and miss-classed resulting from the large overlaps of the gear digital number values. This

classification was performed on a level 4 image with a scale factor of 20 and a function slope of 0.5 and used the mean and standard deviation descriptors. The class descriptions in Figure 31 show the class name and colour used for all of the four-class processes. Segments with any other colour are unclassed segments and still have their original brightness colour from the segmentation process.

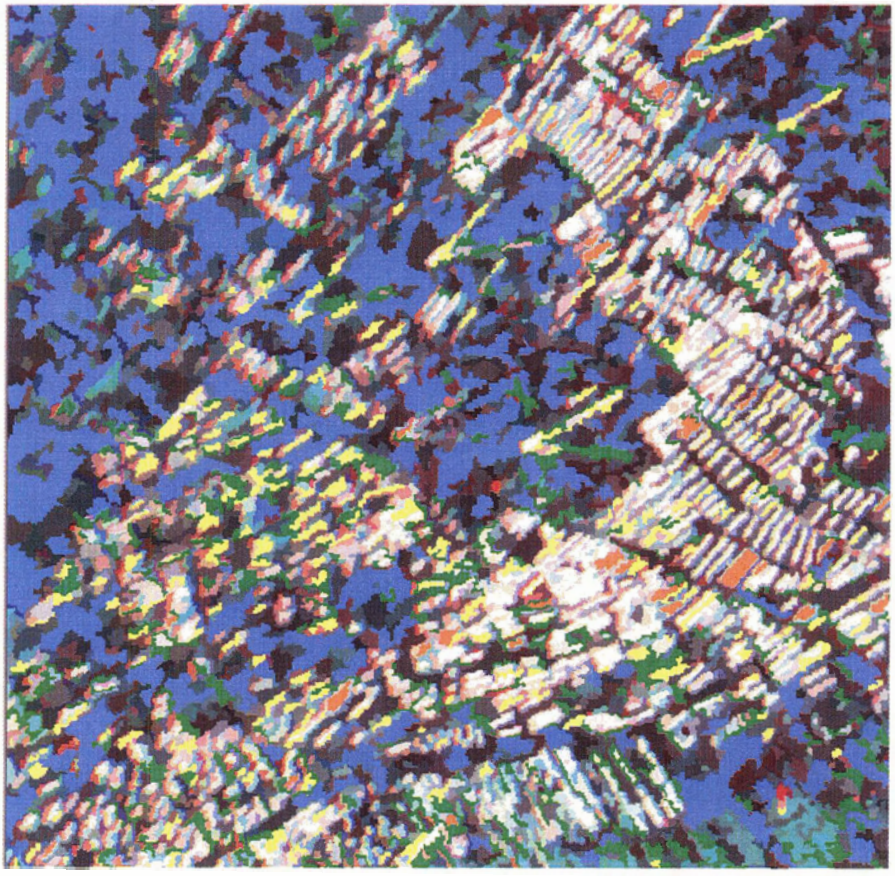

Figure 30 Initial classification using mean and standard deviation as descriptors and a function slope of 0.5 (1:60,000)

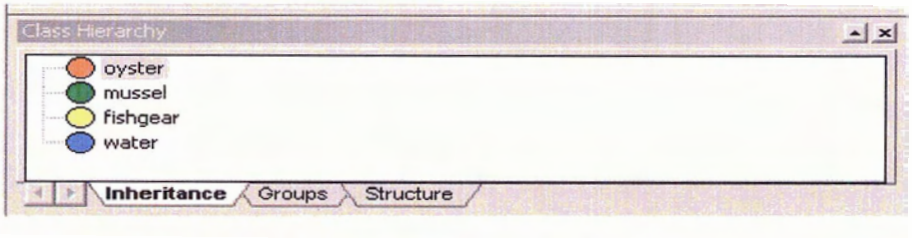

Figure 31 Class descriptions for the four-class trials

Figure 32 displays the results from a further classification trial performed on a level 7 segmentation, where the main direction and rectangular fit shape descriptors were used along with the mean difference to neighbors descriptor and the function slope was increased to 0.7. This classification attempt was the most successful of the attempted four-class tests. Increasing the level of segmentation and the function slope increased the segment size and decreased the distance a segment must be from a sample to be classified, which improved classification results.

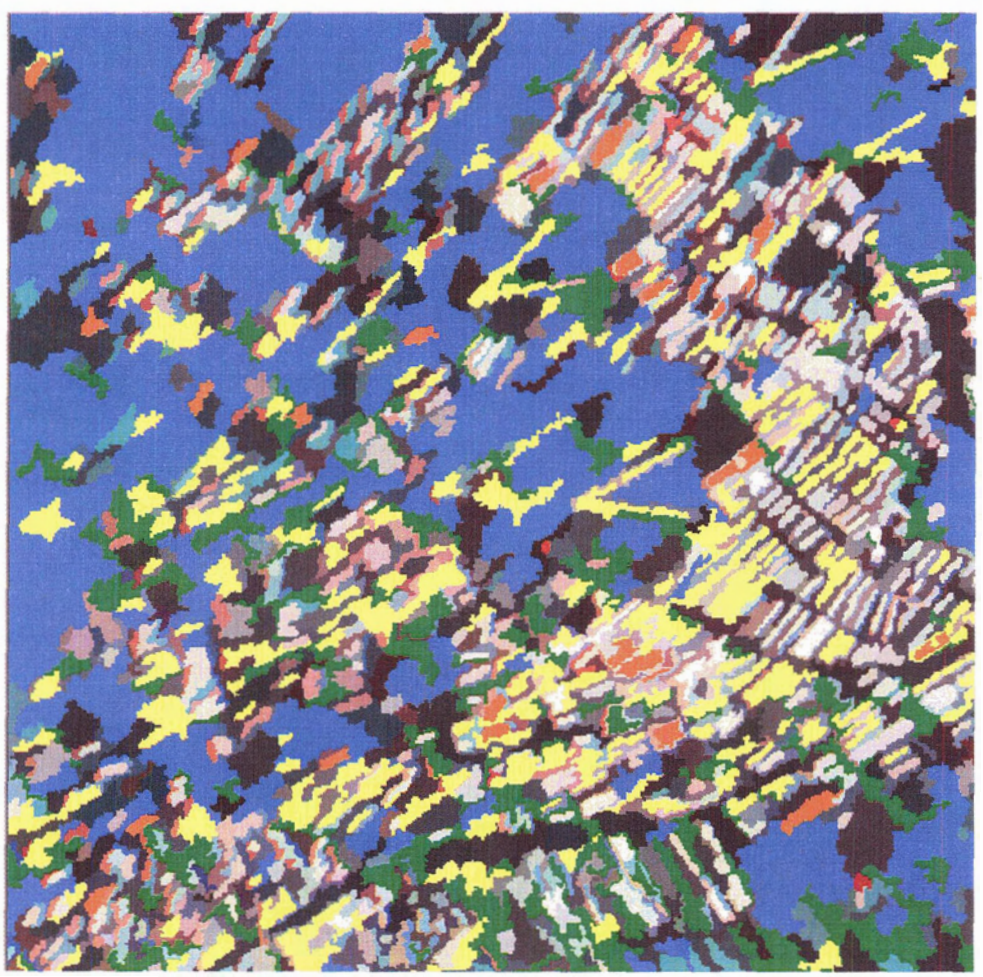

Figure 32 Classification using mean distance to neighbors, main direction and rectangular fit descriptors and a function slope of 0.7 (1:60,000)

As can be seen above, the classification results in Figure 32 show a substantial improvement on the results from the initial classification test shown in Figure 30. However, it is still obvious that the aquaculture and fishing gears are poorly separated from one another at this stage. The larger segments in this latter image help to increase the classification accuracy as fewer segments are confused when the segment-joining threshold increases and fewer segments are formed. The overall accuracy from the classification of Figure 30 was very low at approximately 25%, while the classification improvements leading to the image in Figure 32 presented an accuracy of 36%, still significantly low. These results show that automatic separation of the gears using the above methods is not possible.

In an attempt to improve class separation results, the four original classes were divided into nine, less broad classes, as seen in Figure 33. The narrower ranged

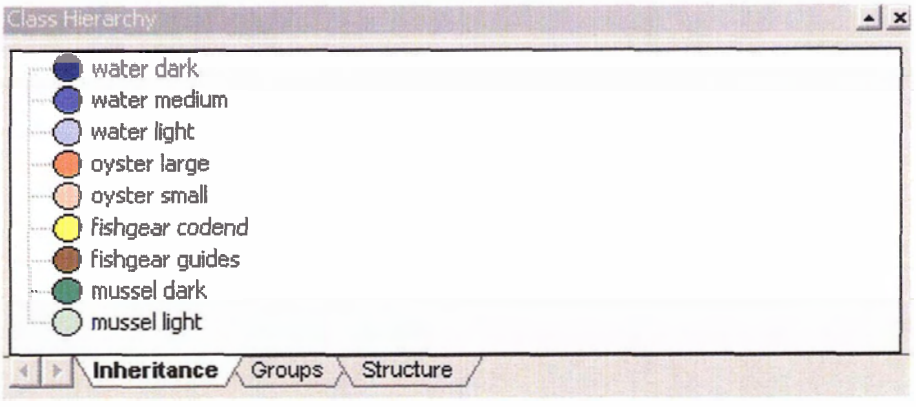

Figure 33 Class descriptions for the nine-class trials

classes improved the results, as some of the digital number overlap between classes was reduced as seen below in Table 17. For example, in the April 8 backscatter data the overlap between the fish gear guides and codends was reduced to the point of separation in the final classification with the codend range being 226 to 248 and the guide range

being 175 to 239. The small overlap remaining between these two classes was made less significant by the rectangular fit shape descriptor also used in the class separation.

Table 17 Mean, standard deviation and colour of the nine classes from the classification results

		08-April-02		17-May-02		26-May-02		10-June-02		06-July-02	
Classes	**Colour**	**Mean**	***Std.Dev***	**Mean**	***Std.Dev***	**Mean**	***Std.Dev***	**Mean**	***Std.Dev***	**Mean**	***Std.Dev***
Water Dark	Dark Blue	84.6	*2.49*	96.5	*7.02*	99.7	*17.1*	122	*9.03*	85.1	*2.11*
Water Medium	Medium Blue	93.7	*2.4*	102	*11.5*	101	*11*	126	*12.4*	94.1	*2.64*
Water Light	Light Blue	115	*9.83*	132	*28.4*	133	*36.4*	150	*28*	116	*9.49*
Oyster Large	Orange	232	*7.93*	230	*14.3*	221	*27.4*	229	*25*	230	*8.53*
Oyster Small	Cream	219	*14.7*	217	*27*	213	*34.6*	217	*30*	215	*24.1*
Fishgear Codend	Yellow	237	*11.6*	221	*21.3*	225	*23.9*	212	*37.7*	230	*12*
Fishgear Guides	Brown	207	*32*	196	*45.2*	189	*54.3*	197	*43.4*	210	*31.8*
Mussel Dark	Dark Green	147	*13.9*	152	*28.4*	157	*42.8*	162	*29.4*	146	*13.6*
Mussel Light	Light Green	217	*21.1*	209	*35.6*	203	*42.5*	207	*37.4*	216	*20*

These new classes were determined through analysis of the shape and spectral characteristics in the segmented image in Figure 28, page 72. A new set of class descriptors was developed for each class by studying the statistical ranges of the classes, as mentioned in section 4.2.2. Figure 34 displays the most accurate nine-class classification, which was performed on the same segmentation image used for the four-class tests as mentioned above.

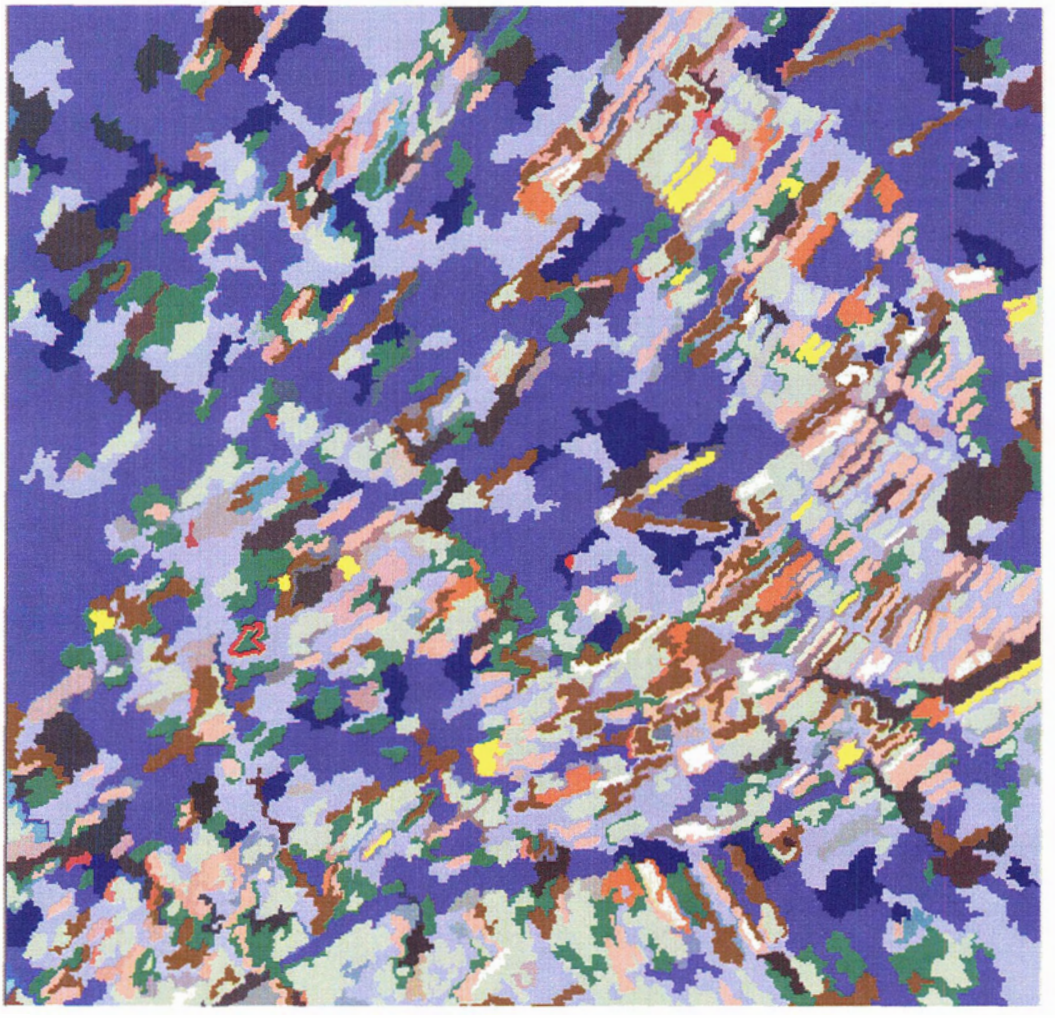

Figure 34 Classification using mean, length, width, mean difference to neighbors, rectangular fit and asymmetry descriptors and a function slope of 0.6 (1:60,000)

Using nine narrower ranged classes improved the classification in that the number of unclassed objects was greatly reduced to only 12%. However, some of the larger unclassed objects in the top left of the image above and one object in the right center, which are obviously water segments by their shape and colour, lead to confusion. In general the water class was successfully classified, as overlap with the gear classes was insignificant. Classification of the fishing gear guides is greatly improved from previous tests, although the majority of the fishing gear codends have been miss-classed as light

mussel gear, as the codends resemble the light mussel gear both spectrally and shape wise. The large oyster gear was very poorly classified as well with only a 10% producer's accuracy as calculated in the following accuracy assessment. Only 12 image objects in total were labeled as large oyster, and objects that should be large oyster were again labeled as light mussel gear. Similarly, although more small oyster gears were classified than the large oyster gear, this class was still misrepresented at 38% accuracy. Again, some small oyster gears were labeled as light mussel because of their backscatter value and some were labeled as fish gear guides because of their shape. The dark and light mussel gears were also miss-classed at accuracies of 57 and 64 percent respectively. The dark mussel was confused for the light water class as can be described by the data in Table 17, where the lower bound of the dark mussel class overlaps with the upper bound of the light water class. Also, a small number of dark mussel objects were classified as fish gear guides. Finally, light mussel objects that were confused in the classification were either classed as small oyster gear, fish gear codends or were unclassed. This classification was the best one of all trials attempted, yet had an overall accuracy of only 51%. Classification accuracy this low does not support the question of using Radarsat-1 imagery to automatically separate the fishing and aquaculture gear types.

5.7 Accuracy Assessment

Accuracy tests available in the image processing software are not acceptable as they only assess the accuracy of classification of the samples, which are chosen because they represent the classes well and so will inflate accuracy calculations (Niemann, 2003). For this reason a random stratified sample of the images was performed and error

matrices were created for both the four and nine-class tests to assess the classification accuracies.

The reference image, the 1100 by 1100 pixel filtered image subset used for the segmentation and classification tests, was compared to the best final classification images for the assessment. These images were geocoded, which allowed the selection of the same location on each image for sample image pixel labeling and classification segment labeling in the tallying of the error matrix numbers. Figures 35 displays the reference image used in the assessment with the overlain stratified grid and samples. Figure 36 below provides a zoom view at the same location on the three images to display the random samples within the stratified grid.

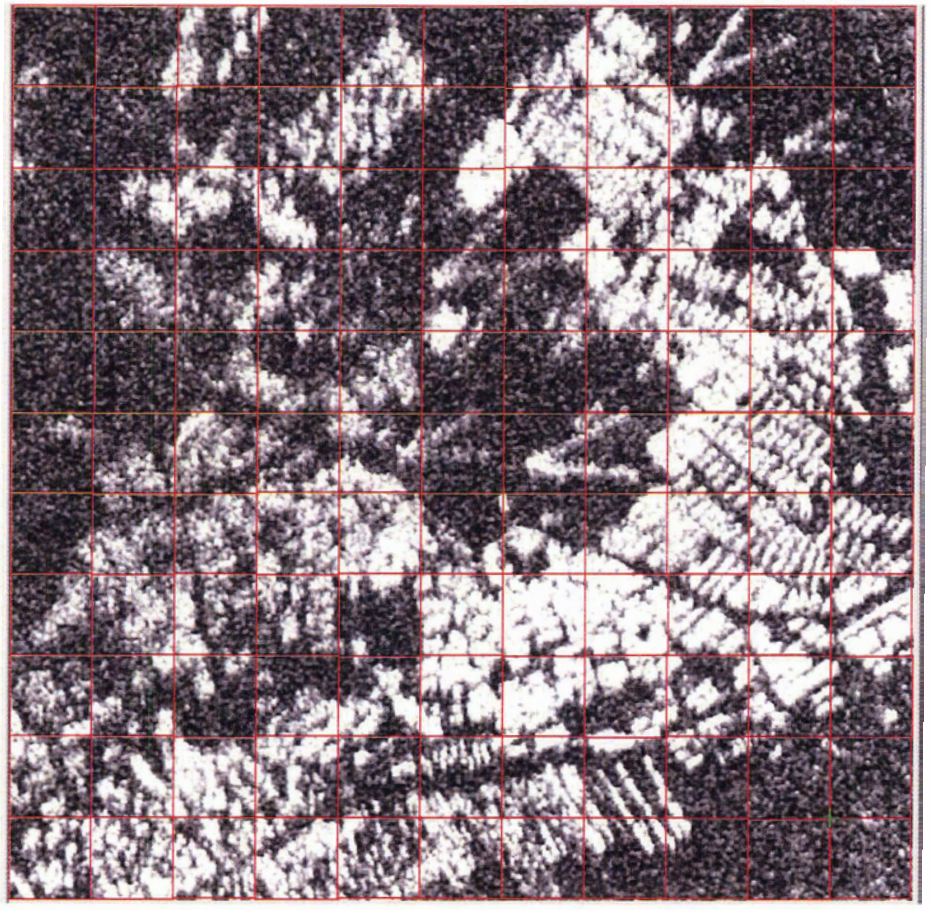

Figure 35 Reference image with stratified 100 by 100 pixel grid and samples (1:60,000)

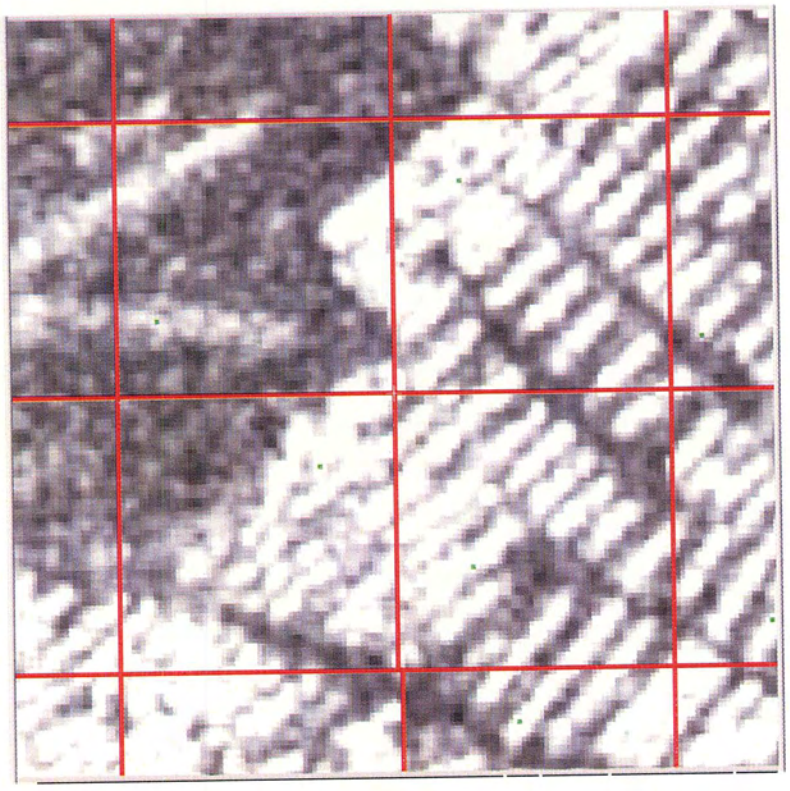

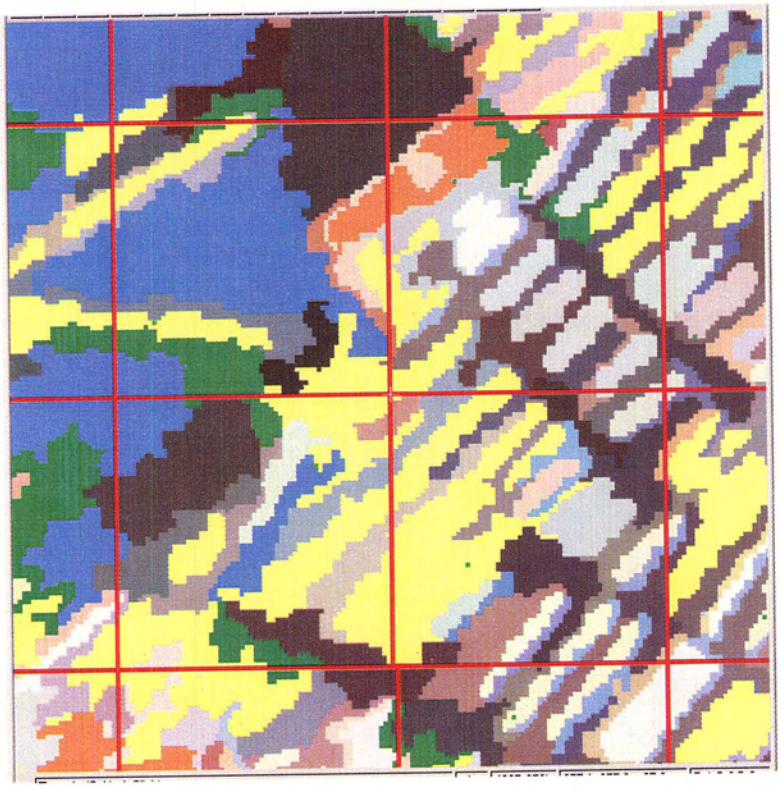

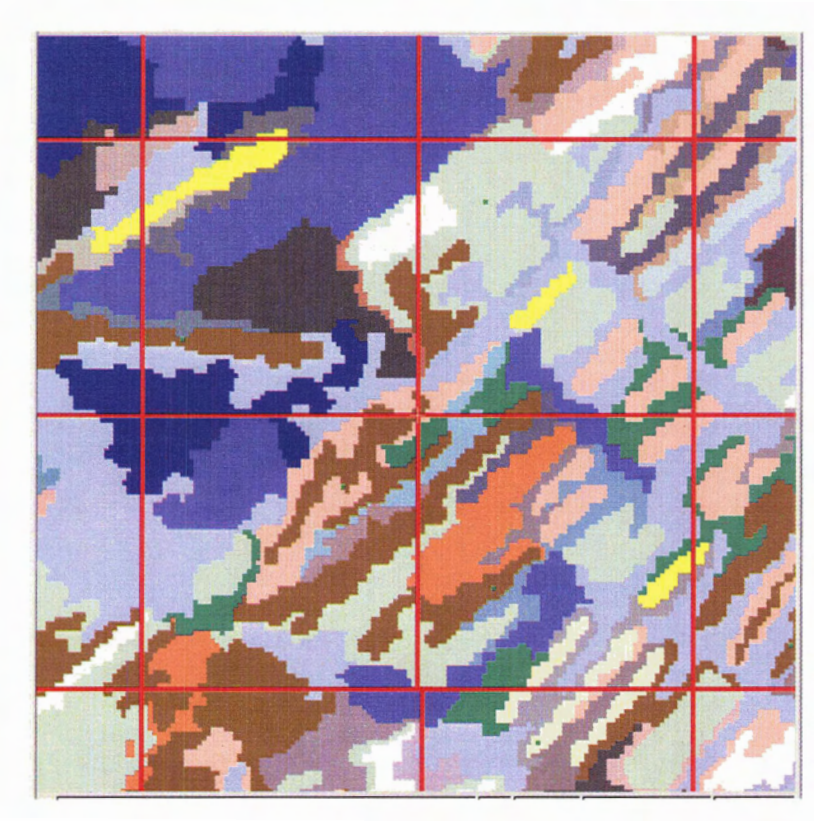

Figure 36 Zoom view showing the same location on the reference and both classification images (four-class and nine-class respectively), single green pixel in each grid is a sample (1:2000)

As can be seen in the above images, a stratified grid of 100 by 100 pixels was created as a segment on the image files and one random sample was chosen from within each grid to assess the classification accuracy. It is also apparent that more segments were left unclassed in the four-class test, which will be quantified from the following error matrix data. Table 18 displays the error matrix data translated from the two images for the four-class test and Table 19 contains the data for the nine-class test. Legends for the two matrices are found below the respective table.

Table 18 Error matrix for the four-class test

		Reference data					
		O	**M**	**F**	**W**	**U**	**Total**
Classification data	**O**	**4**	0	0	0	0	4
	M	6	**6**	0	4	0	16
	F	10	7	**8**	0	0	25
	W	0	0	0	**26**	0	26
	U	27	14	3	6	**0**	50
	Total	47	27	11	36	0	*121*

Legend: O = oyster, M = mussel, F = fishgear, W = water, U = unclassed
Overall Accuracy: 4+6+8+26+0 = 44/121 = 0.36 = 36%

Table 19 Error matrix for the nine-class test

		Reference data										
		DW	**MW**	**LW**	**LO**	**SO**	**FC**	**FG**	**DM**	**LM**	**U**	**Total**
Classification data	**DW**	**4**	0	0	0	0	0	0	0	0	0	4
	MW	2	**17**	1	0	0	0	0	0	0	0	20
	LW	0	0	**8**	0	0	0	0	1	0	0	9
	LO	0	0	0	**2**	0	0	0	0	0	0	2
	SO	0	0	0	5	**13**	0	0	0	1	0	19
	FC	0	0	0	0	1	**0**	0	0	0	0	1
	FG	0	0	0	4	3	1	**7**	0	1	0	16
	DM	0	0	0	0	2	0	1	**4**	0	0	7
	LM	0	0	0	8	13	1	0	0	**7**	0	29
	U	3	1	1	2	2	1	0	2	2	**0**	14
	Total	9	18	10	21	34	3	8	7	11	0	*121*

Overall Accuracy: 4+17+8+2+13+0+7+4+7+0 = 62/121 = 0.51 = 51%

Legend:
DW = dark water
MW = medium water
LW = light water
LO = large oyster
SO = small oyster
FC = fishgear codend
FG = fishgear guide
DM = dark mussel
LM = light mussel

As is common in error matrix format, the columns in the tables display the reference data and the rows display the classification data (Congalton and Green, 1999). The far right column and the last row display the matrix totals, while the penultimate column and row display the unclassed samples. The error matrix represents the classification accuracy as well as displays errors of classification commission, where a pixel is included in a category to which it does not belong; and errors of omission, where a pixel is excluded from a category to which it really belongs (Congalton and Green, 1999). The error matrix is also used to calculate overall accuracy of the classification and producer's and user's accuracies of the individual classes (PCI Geomatica, 2000). The overall accuracy is calculated by dividing the sum of the major diagonal (shown in bold numbers in the above tables) of the matrix by the total number of sample units in the lower right square (shown in italics) and multiplying it by 100 (Congalton and Green, 1999). Congalton and Green (1999) point out that producer's and user's accuracies represent individual category accuracies rather than total classification accuracy. Dividing the major diagonal value in a row or column by the total at the end of that respective row or column and multiplying it by 100 can calculate the producer's (column) and user's (row) accuracies.

The overall accuracy for the four-class test was 36%, whereas the overall accuracy for the nine-class test was improved at 51%. Considering the apparent inability to separate the gear signatures from one another, a final accuracy test to quantify the separation of the gear from the water background was calculated using the nine-class error matrix data. The error matrix is seen below in Table 20. The overall accuracy for gear separation from water was 88%, as 106 of the 121 samples were correctly classified. This suggests that low tide Radarsat-1 imagery can very successfully detect the various fishing and aquaculture structures in tropical regions of the world. Calculations for the above-mentioned producer and user accuracy tests are included in Appendix II.

Table 20 Error matrix with 2 classes, water and gear

		Reference data			
Classification data		**water**	**Gear**	**unclassed**	**Total**
	water	**32**	1	0	33
	gear	0	**74**	0	74
	unclassed	5	9	**0**	14
	total	37	84	0	*121*

Overall Accuracy: 32+74+0 = 106/121 = 0.88 = 88%

5.8 Summary

This chapter displayed and discussed the results of various image processing techniques that were applied in an attempt to separate the backscatter signatures of coastal fishing and aquaculture gears in the Gulf of Thailand. It also provided an accuracy assessment for the image classifications performed. The following chapter discusses future research that may lead to improved gear signature separation.

Chapter 6

6.0 Conclusion

The purpose of this study was to determine if Radarsat-1 imagery could be used to detect and monitor stationary fishing gear and aquaculture gears on the eastern Gulf of Thailand. Upon detection of these gears, various image processing techniques were applied to single images and multi-image composites to test their ability to separate the backscatter signals of three main gear types found in the region: stationary fishing gears, oyster racks and mussel stakes. If these gears can be automatically separated in the radar imagery, then resource managers can monitor changes in coastal fishing and aquaculture activities without needing the personnel and equipment to survey remote coastal areas.

The first objective of this research was to determine if fishing and aquaculture gears in near-shore waters composed of bamboo and palm stakes could be detected by radar satellite imagery from Radarsat-1. These gears all protrude above the water surface at low tide levels, creating corner reflectors that intercept the incoming radar signal and return a backscatter signal to the satellite. However, the structures are not solid, but filamentous, so it was uncertain if the strength of the signals would be strong enough to be detected. This research determined that the gear structures present in the study area all return a significant backscatter signal detectable by the Radarsat-1 fine beam mode sensor. The detection of the gears does not require image processing if image acquisition occurs during low tide levels and when the sea surface is relatively calm (surface waves less than 2 meters). Full resolution views of the images displayed the gears quite clearly before any processing had been applied.

The second research objective questioned if the different gear types in the study area had distinct spatial or textural patterns that would make signature separation possible. As seen in chapter two of this thesis, each of the five gears in the area has a different structure, shape and location. Visually, the gears could be differentiated both in the field and on the satellite imagery. The challenge then, was to determine if image processing techniques could numerically separate the gear signals, allowing for automatic gear separation.

Two image processing techniques, segmentation and classification, were tested to determine their ability to separate the gear signatures. Results from image segmentation trials proved that all of the gears in the study site could be visually separated. However, numeric gear separation was low because the oyster signature overlapped greatly with the fishing gear codend signature and the mussel signature overlapped with the fishing gear codend and oyster signatures. These digital number overlaps lowered the possibility of gear separation at the segmentation level and lead to testing classification techniques to attempt gear separation.

Segment classification utilizing both the spectral (backscatter) and spatial (shape) characteristics of the image segments was also unsuccessful at automatically separating the gear signatures to an acceptable level. The highest classification accuracy attained for gear separation was 51%. However, this accuracy level was including the water class, which would have raised the true gear separation accuracy to some extent, as the water class separates well from the gear classes as seen in Figure 29. The multi-class classification trials did not provide acceptable automatic gear separation results, again because of the backscatter signature overlap.

A further research objective was to determine if multi-angle imagery was necessary for identifying fishing and aquaculture gears and if any one incidence angle image improved the differences in gear signature separation. The five images used for the project were acquired from incidence angles F2, F4 and F5, F2 being a steep angle (39.3-42.3) and F4 (43.6-46.0) and F5 (45.3-47.8) being shallower angles. The textural patterns in the images were similar and all angles contain useful information; however, the shallower angled images (F4 and F5) provided more information for the gear types that were less dense in structure, such as the blood cockle enclosures and the guides for the stationary fishing gears. Multi-angle imagery is not required for fishing and aquaculture gear detection or separation as all images provided adequate information for manual separation of the most prevalent gear types, though the shallower angled images may improve detection of finer structured gears.

The final objective was to determine if multitemporal imagery was important in detecting and separating the features of interest. The images were acquired on different dates throughout the summer of 2002 to increase the amount of data available for analysis. Although some image dates provided more information than others, it was not determined necessary to analyze multitemporal imagery for this project, as all of the gears studied are stationary and have relatively long term life spans. The varied amounts of gear information in the images were related to the different surface wave heights and incidence angle, not multi-temporal imaging. Low tides and relatively calm waters were the most important factors affecting detection of the various gears. However, multitemporal imagery can be useful in detecting gear removal or construction, as some of the gears are seasonal depending on the species of interest. Similarly, during the

stormy season multitemporal imagery may be necessary to capture data during calm sea conditions.

In summary, manual separation of the features of interest in Radarsat-1 imagery performs better than automatic separation. It is possible to either filter or segment out the gears to a point where they can be manually classified with acceptable accuracy using field descriptions; whereas, automatic classification of the various types of gear has low accuracy, at approximately 51%. The similar composition and structures of the gears, which lead to similar backscatter values, do not allow for automatic gear separation in this case. However, a more general classification, separating gear from water can be performed automatically with 88% accuracy, which is very useful in the case of gear detection and coastal monitoring.

Further research toward the separation of stationary fishing and aquaculture gears in tropical coastal waters may prove more successful on higher resolution imagery, as gear shape differences would become more defined. The finer resolution imagery that will be available from Radarsat-2 (3 meter) may add more backscatter information and perhaps allow better signature separation, however this will be at a total surface coverage cost. With less ground area covered in an image, satellite monitoring of a country's coastline becomes more expensive as more images are required to encompass the entire area of interest.

Also regarding Radarsat-2, this imaging satellite will have multi-polarized capabilities. Adding the possibility of vertical or cross-polarized data to the investigation may supply backscatter or spatial information about the gears that was not available with the horizontally polarized images, which may allow for better signature separation.

Further, some of the gear types in the study area such as mussel and blood cockle gear are fully submerged at the highest tide level, while oyster and stationary fishing gears still protrude from the water surface. Acquiring imagery from both high and low tide levels may help to partially separate the gear types that have a different height structure. In this case, the signature overlap between the mussel and oyster class may be eliminated.

This study proposes a methodology that has large potential for monitoring coastal fishing and aquaculture activities in tropical countries where heavy cloud cover is prevalent. Automatic detection of all of the gear types in the study area was successful and highly accurate on the Radarsat-1 fine beam mode imagery. Manual classification of the different gears on a filtered image is possible and accurate when compared to field notes. However, automatic separation of the fishing and aquaculture gears found in the study area results in low accuracies with the data and software available. The backscatter values of the different gear types have significant overlap, which increases error in the classification.

The 88% accurate automatic detection of the gears provides coastal resource managers with an avenue to effectively determine areas of fishing and aquaculture activity, rendering Radarsat-1 fine beam mode imagery a useful decision making tool.

References

Alexander, L.A. and M. R. Inggs. 1996. Synthetic aperture radar for remote sensing. *South African Journal of Science*, 92, 106–109.

Baatz, M. and A. Schäpe. 2000. Multiresolution segmentation: an optimization approach for high quality multi-scale image segmentation. *AGII Symposium*, Salzburg, Austria.

Bhatiyasevi, U. 1997. Marine resources and fisheries in the exclusive economic zones of Thailand. *Fishery Resources and State of Stocks Exploitation in the Waters of the Gulf of Thailand, East Coast of Peninsular Malaysia and Andaman Sea.* South East Asian Fisheries Development Center (SEAFDEC), Bangkok, Thailand. 90p.

Brohamonda, P., K. Mutarasint, T. Chongpeepien, S. Amornjaruchit. 1988. Oyster culture in Thailand. In: *Bivalve Mussel Culture Research in Thailand.* E.W. McCoy and T. Chongpeepien (Ed.). Department of Fisheries, Bangkok, Thailand. 31-39p.

Bruniquel, J. and A. Lopes. 1997. Multi-variate optimal speckle reduction in SAR imagery. *International Journal of Remote Sensing*, 18(3), 603-627.

Campbell, F.H.A. 1987. *Introduction to Remote Sensing.* Guildford Press, NY. 374p.

Campbell, F.H.A., R.A. Ryerson, and R.J. Brown. 1995. GlobeSAR: a Canadian radar remote sensing program. *Geocarto International*, 10(3), 3-7.

CCRS, Canada Centre for Remote Sensing. 2001. Radarsat Overview. http://www.ccrs.nrcan.gc.ca/ccrs/tekrd/radarsat/specs/radovere.html

Chalermwat, K. and R.A. Lutz. 1989. Farming the green mussel in Thailand. *World Aquaculture*, 20(4), 41-46.

CIA. The World Factbook. 2003. http://www.cia.gov/cia/publications/factbook/geos/th.html

Congalton, R.G and K. Green. 1999. *Assessing the Accuracy of Remotely Sensed Data: Principles and Practices.* CRC Press, Boca Raton, Florida. 137p.

Corbley, K.P. 1985. RADARSAT: meeting the needs of users worldwide. *Geocarto International*, 10(3), 87-91.

Costa, M. 2000. Net Primary Productivity of Aquatic Vegetation of the Amazon Floodplain: A Multi-SAR satellite Approach. *University of Victoria*, Ph.D. Thesis. 230p.

Costa, M. 2003. Personal Communication. Department of Geography, University of Victoria, Victoria, British Columbia.

Definiens Imaging. 2003. eCognition: Object Oriented Image Analysis. Version 3.0, Munich, Germany.

Filion, R. 2003. Evaluation of RADARSAT-1 for Monitoring and Mapping Land Use / Land Cover in Thailand. *University of Victoria*, MSc. Thesis. 278 p.

Forster, B. 1996. Current advances in radar remote sensing research and its application in South East Asia, *Geocarto International*, 11(4), 3-10.

Freeman, A. 1992. SAR calibration: an overview. *IEEE Transaction of Geoscience and Remote Sensing*, 30(6), 1107-1121.

Frulla, L. A., Milovich, J.A. and Gagliardinis, D.A. 2000. Automatic computation of speckle deviation in SAR images. *International Journal of Remote Sensing*, 21(15), 2883-2899.

Fung K.A. and F.T. Ulaby 1983. Chapter 4: Matter-Energy Interaction in the Microwave Region. In: *Manual of Remote Sensing.* Colwell, N., D.S. Simonett, F.T. Ulaby (Eds.). John Wiley & Sons Inc., NY. 866p.

Gineste, P. 1999. A simple, efficient filter for multitemporal SAR images. *International Journal of Remote Sensing*, 20(13), 2565-2576.

Gonzalez, R.C. and Wintz, P. 1987. *Digital Image Processing.* Addison-Wesley, MA. 503p.

Gower, J. and S. Skey. 2000. Evaluation of RADARSAT scanSAR for observing wind, slicks and fish-boats. *Canadian Journal of Remote Sensing*, 26(6), 484-493.

Henderson, F.M. and A.J. Lewis. 1998. *Principles and Applications of Imaging Radar.* John Wiley & Sons Inc., NY. 866p.

Hogda, K.A and Eirik Malnes. 2002. Use of Radarsat F5 images for detection and positioning of fish cages. *Geoscience and Remote Sensing Symposium, IGARSS '02Proceedings*, 5, 3047 -3049.

Hydrographic Department, Royal Thai Navy. 2002. *Tide Tables Thai Waters – Mae Nam Chaophraya, Gulf of Thailand and Andaman Sea.* 84p.

Jensen, J.R. 1996. *Introductory Digital Image Processing.* Prentice Hall Inc., NJ. 316p.

Jensen, J.R. 2000. *Remote Sensing of the Environment: an Earth Resource Perspective.* Prentice Hall, NJ. 544p.

Jiang, Q., E. Aitnouri, S. Wang, and D. Ziou. 2000. Automatic detection for ship target in SAR imagery using PNN-model. *Canadian Journal of Remote Sensing*, 26(4), 297-305.

Johannessen, J.A., L.P. Lars, O.M. Johannessen, G. Evensen, B. Hackett, L.H. Pettersson, P.M. Haugan, S. Sandven and R. Shuchman. 1993. Monitoring and modeling of the marine coastal environment. *Photogrammetric Engineering & Remote Sensing*, 59(3), 351-361.

KartlabUU. 2003. Oddens' Bookmarks: The Fascinating World of Maps and Mapping. http://www.lib.utexas.edu/maps/middle_east_and_asia/thailand_provinces_88.jpg

Kourti, N., I. Shepherd, G. Schwartz, and P. Pavlakis. 2001. Integrating spaceborne SAR imagery into operational systems for fisheries monitoring. *Canadian Journal of Remote Sensing*, 27(4), 291-305.

Kushwaha, S.P.S., R.S. Dwivedi and B.R.M. Rao. 2000. Evaluation of various digital image processing techniques for detection of coastal wetlands using ERS-1 SAR data. *International Journal of Remote Sensing*, 21(3), 565-579.

Lillesand, T.M. and R.W. Kiefer. 1994. *Remote Sensing and Image Interpretation*. 3rd ed., John Wiley & Sons Inc., NY. 750p.

Lillesand, T.M. and R.W. Kiefer. 2000. *Remote Sensing and Image Interpretation*. 4th ed., John Wiley & Sons Inc., NY. 724p.

Loos, E. November 19, 2001. Geography 322 webpage, University of Victoria. http://www.geog.uvic.ca/geog322/

Lopes, A., R. Touzi and E. Nezry. 1990. Adaptive speckle filters and scene heterogeneity. *IEEE Transactions on Geoscience and Remote Sensing*, 28(6), 992-1000.

Lutz, R.A, K. Chalermwat, A. J. Figueras, R. G. Gustafson and C. Newell. Mussel aquaculture in marine and estuarine environments throughout the world. In: *Estuarine and Marine Bivalve Mollusk Culture*. W. Menzel (Ed.). CRC Press, Boca Raton, Florida, USA, 57-97p.

Maps.com. 2003. Thailand Base Printable Map. http://www.maps.com/cgibin/magellan/Map_Store_Printable_Maps_AsiaMDCP_P_THA

Mumby, P.J., E.P. Green, A.J. Edwaeds, and C.D. Clark. 1999. The cost-effectiveness of remote sensing for tropical coastal resources assessment and management. *Journal of Environmental Management*, 55, 157-166.

Niemann, K.O. 2003. Personal Communication, PhD. Department of Geography, University of Victoria, Victoria, British Columbia.

Okawara, M., A. Munprasit, Y. Theparoonrat, P. Masthawee and B. Chokesanguan. 1995. *Fishing Gear and Methods In Southeast Asia: I. Thailand*, DSO-SEAFDEC Project, 255p.

Oliver, C. and S. Quegan. 1998. *Understanding Synthetic Aperture Radar Images*. 1st ed., Artech House Inc., MA. 478p.

Pasqualini, V., J. Iltis, N. Dessay, M. Lointier, O. Guelorger, and L. Polidori. 1999. Mangrove mapping in north-western Madagascar using SPOT-XS and SIR-C radar data. *Hydrobiologia*, 413, 127-133.

Pauley, D., V. Christensen, J. Dalsgaard, R. Froese, and F. Torres. 1998. Fishing down marine food webs. *Science*, 279, 860-863.

PCI Geomatica, Version 8.2. 2000. Richmond Hill, Ontario, Canada.

Rajesh, K., C.V. Jawahar, S. Sengupta and S. Sinha. 2001. Performance analysis of textural features for characterization and classification of SAR images. *International Journal of Remote Sensing*, 22(8), 1555-1569.

Raney, R.K. 1998. Radar fundamentals: technical perspective. In: *Principles and Applications of Imaging Radar*. Henderson, F.M. and Lewis A.J. (Eds.). John Wiley and Sons Inc., New York. 9-130p.

Rees, W.G. and J.F. Satchell. 1997. The effect of median filtering on synthetic aperture radar images. *International Journal of Remote Sensing*, 18(13), 2887-2893.

Richards, J.A and X. Jia. 1999. *Remote Sensing Digital Image Analysis*. 3rd ed., Springer – Verlag: Berlin. 363p.

Royal Thai Survey Department. 1990. 1:50,000 map sheet. Bangkok, Thailand.

Sabins, F.F. 1987. *Remote Sensing: Principles and Interpretation*. 2nd ed., W. H. Freeman and Company: NY. 449p.

Sabins, F.F. 1997. *Remote Sensing Principles and Interpretation*. 3rd ed., W.H. Freeman and Company: NY. 494p.

Saraya, A. 1982. *Bivalve Culture In Asia and the Pacific: proceedings of a workshop held in Singapore, 16-19 February 1982*. Eds. F. B. Davy and M. Graham, 73p.

SEAFDEC and Kasetsart University. 1997. Attitude of small-scale fishermen toward the fishing right system in Chantaburi Province. Proceedings of the Regional Workshop on Coastal Fisheries Management Based on Southeast Asian Experience, Chiang Mai, Thailand, November 19-22, 1996. SEAFDEC, Samut Prakarn Thailand, 198p.

Segl, K. and H. Kaufmann. 2001. Detection of small objects from high-resolution panchromatic satellite imagery based on supervised image segmentation. *IEEE Transactions on Geoscience and Remote Sensing*, 39(9), 2080-2083.

Smith, D.M. 1996. Speckle reduction and segmentation of synthetic aperture radar images. *International Journal of Remote Sensing*, 17(11), 2043-2057.

Suvapepun, S. 1997. Environmental aspects of responsible fisheries in the Gulf of Thailand. In *Environmental Aspects of Responsible Fisheries*. Proceedings of the APFIC Symposium, Seoul, Korea, October 15-18, 1996. FAO, Bangkok, Thailand, 168p.

Szuster, B. 2001. Personal communication. Field Manager for Thailand Aquaculture Management Project. Department of Geography, University of Victoria, Victoria, British Columbia.

Touzi, R. 1999. Taking The Speckle Out of SAR: The Multi-Resolution Filter. *RSIC* (Remote Sensing In Canada, on-line). 27(1). http://www.ccrs.nrcan.gc.ca/ccrs/com/rsnewsltr/2701/2701ra2_e.html

Ulaby, F.T. and I. Dobson. 1987. *Handbook of Radar Scattering Statistics for Terrain*. Artech House, Inc. U.S.A., 357p.

Vakily, J.M. 1989. *The Biology and Culture of Mussels of the Genus Perna*. International Center for Living Aquatic Resources Management, Manila, Philippines, 63p.

Wackerman, C.C., K.S. Friedamn, W.G. Pichel, P. Clemente-Colon, and X. Li. 2000. Automatic detection of ships in RADARSAT-1 SAR imagery. *Canadian Journal of Remote Sensing*, 27(4), 371-378.

Appendix I

GPS Data Tables From Field Study

RADARSAT GPS SURVEY April 23, 2002

Surface Wind Conditions: 20-30 kph
Wave Conditons: 0.5 meter

Photo #	Northing	Easting	Comments
1	13-15-16.8	100-54-51.2	mussel stakes looking N
2	13-15-16.8	100-54-51.2	fish trap looking SE
3	13-15-16.8	100-54-51.8	fish trap looking NW
4	13-15-07.4	100-54-57.4	fish trap looking SW
5	13-15-58.1	100-53-58.9	fish trap looking SE
6	13-18-25.6 to 43.8	100-53-52.5 to 54-09.2	mussel stakes running N/S
7	13-19-01.4	100-54-39.1	oyster rafts looking E
8	13-19-22.9	100-54-37.6	oyster rafts looking N
9	13-19-22.9	100-54-37.6	oyster rafts looking E
10	13-19-34.8	100-54-56.3	jellyfish processing shed
11	13-19-41.0	100-54-55.1	oyster rafts looking E
12	13-19-41.0	100-54-55.1	oyster rafts looking E
13	13-19-41.0	100-54-55.1	oyster rafts looking E
14	13-20-18.2	100-55-09.4	30 m. fisheries patrol boat near oyster rafts
15	13-20-28.3	100-55-25.0	oyster rafts looking N
16	13-20-43.5	100-55-33.4	oyster rafts looking N
17	13-21-00.5	100-55-25.8	oyster rafts looking N
18	13-21-20.3	100-55-31.0	mussel stakes and house
19	13-21-40.5	100-55-17.0	mussel stakes looking NE
20	13-22-08.9	100-55-42.5	fish trap looking NE (200 m. away)
21	13-22-08.9	100-55-42.5	fish trap looking N
22	13-22-42.6	100-55-45.3	2 fish traps looking NE toward power plant
23	13-23-05.2	100-55-36.5	fish trap looking N
24	13-23-15.3	100-55-32.5	big oyster rack farm looking north
25	13-23-27.0	100-54-58.3	2 fish traps looking N
26	13-23-09.3	100-54-21.7	fish trap looking N (another in distance to N)
27	13-23-09.3	100-54-21.7	several traps toward W (1-2 km)
28	13-22-43.1	100-54-39.9	fish trap looking N
29	13-22-29.9	100-54-47.9	fish trap looking N
30	13-22-05.6	100-53-54.8	fish trap looking W
31	13-22-05.6	100-53-54.8	several traps toward W (1-2 km)
32	13-21-47.3	100-53-39.4	several traps toward W (1-2 km)
33	13-21-25.0	100-53-20.0	4 fish traps toward W (3 in distance) *estimate
34	13-20-56.7	100-53-13.4	fish trap in distance toward W (about 1 km)
35	13-20-35.0	100-53-08.2	fish trap

RADARSAT GPS SURVEY May 16, 2002

Tide Level May 17 - 0.85m
Surface Wind Conditions: 40-50 kph
Wave Conditons: 0.5 - 1 meter

Photo #	Northing	Easting	Comments
1	13-21-35.4	100-55-45.7	oyster racks facing SE
2	"	"	oyster racks facing NW
3	13-22-06.4	100-56-07.1	oyster platforms facing NE
4	13-22-45.1	100-56-32.1	staionary fishing gear
5	"	"	"
6	13-22-54.8	100-56-50.5	staionary fishing gear
7	13-23-13.0	100-57-08.9	oyster platforms facing N
8	13-25-53.8	100-57-21.0	large shrimp pen facing NE (corner of upper gulf)
9	13-28-25.2	100-58-15.1	seabass farm (some grouper too)
10	"	"	"
11	"	"	"
12	13-29-22.0	100-58-44.2	seabass farm
13	13-24-43.7	100-56-30.6	oyster racks (large group of them)
14	"	"	"
15	"	"	"
16	"	"	"
17	13-24-15.6	100-56-15.1	stationary fish trap
18	"	"	stationary fish trap with wings
19	13-24-09.9	100-56-09.7	green mussel stakes facing SW
20	13-24-22.7	100-55-21.7	abandoned fish trap
21	13-23-39.0	100-55-11.0	oyster racks
22	13-22-42.0	100-55-42.3	oyster racks
23	13-22-35.6	100-55-42.0	mussel stakes
24	13-21-59.6	100-55-57.3	growing mussel on oyster rack with horizontal lines
25	"	"	"
26	13-21-01.1	100-55-50.0	oyster racks facing SW (many)
27			oysters growing on cement posts
28			oysters growing on cement posts
29	13-18-37.3	100-53-47.6	green mussel stakes

RADARSAT GPS SURVEY JUNE 14, 2002

Tide Level June 14 - 1.3 to .5
Wind Conditions - 15 to 20 kph
Wave Conditions - 0.25 m

Photo #	Northing	Easting	Comments
roll 3 of film			
17	13-22-47.6	100-54-30.7	stationary fish gear
18	13-23-14.3	100-53-58.3	stationary fish gear
19	"	"	"
20	13-23-56.7	100-54-36.8	staionary fishing gear
21	"	"	"
22	13-23-55.2	100-52-17.2	staionary fishing gear
23	"	"	"
24	13-22-50.2	100-49-38.1	stationary fish gear
25	"	"	"
roll 4 photo 1	"	"	"
4	13-16-03.6	100-53-47.4	stationary fish gear
5	"	"	"
6	"	"	"
7	13-15-03.8	100-53-43.1	stationary fish gear
8	"	"	"
10	13-15-17.3	100-54-40.0	stationary fish gear

Radarsat GPS Survey July 6, 2002

10:00 - 12:30 am
Surface Wind Conditions : 15-20 km/h
Wave Conditons: 0.5 meter

roll 5

Photo #	Northing	Easting	Comments
1	13-15-53.0	100-54-51.9	green mussel stakes (N end)
	13-15-42.6	100-54-53.1	same (South end of area)
2	13-15-41.6	100-54-44.0	green mussel stakes
3	13-15-25.6	100-54-08.0	stationary fish gear
4	"	"	"
5	13-15-08.0	100-53-42.7	stationary fish gear
6	"	"	"
7			waves behind boat
8	13-10-50.4	100-54-30.1	stationary fish gear
9	13-10-02.6	100-54-18.4	stationary fish gear
10	"	"	"
11	13-09-46.0	100-54-04.9	stationary fish gear
12	13-09-35.5	100-53-31.8	stationary fish gear
13	13-09-28.1	100-53-01.3	large ships docked at Siracha pier
14	"	"	"
15	13-09-57.5	100-52-26.2	large ship out from dock
16	13-10-50.4	100-54-09.6	stationary fish gear

RADARSAT GPS Survey July 9, 2002

10:00 - 2:00 am
Surface Wind Conditions : 15-20 km/h
Wave Conditons: 0.5 meter
end roll 5 to roll 6

Photo #	Northing	Easting	Comments
17	13-10-42.3	100-55-00.6	boat dock looking to longline gear
18	"	"	"
19	"	"	"
20	"	"	"
21			stationary fish gear west of dock (July 6)
22	13-21.09	100-51.29	stationary fish gear
23	"	"	"
roll 6 - 1	13-22.56	100-50.26	stationary fish gear
2	13-22.77	100-49.67	stationary fish gear
3	13-22.98	100-49.12	stationary fish gear
4	13-23.25	100-48.62	stationary fish gear
5	13-24.78	100-47.21	stationary fish gear

Appendix II

Accuracy Assessment Calculations

A. Calculations for the Four-class Test

		Reference data					
		O	**M**	**F**	**W**	**U**	**Total**
Classification data	**O**	**4**	0	0	0	0	4
	M	6	**6**	0	4	0	16
	F	10	7	**8**	0	0	25
	W	0	0	0	**26**	0	26
	U	27	14	3	6	**0**	50
	Total	47	27	11	36	0	*121*

Total of the major diagonal = 4 + 6 + 8 + 26 + 0 = 44

Overall Accuracy = 44/121 = 0.363 x 100 = 36%

Producer's Accuracy
O = 4/47 x 100 = 9%
M = 6/27 x 100 = 22%
F = 8/11 x 100 = 73%
W = 26/36 x 100 = 72%

User's Accuracy
O = 4/4 x 100 = 100%
M = 6/16 x 100 = 38%
F = 8/25 x 100 = 32%
W = 26/26 x 100 = 100%

B. Calculations for the Nine-class Test

		Reference data										
		DW	**MW**	**LW**	**LO**	**SO**	**FC**	**FG**	**DM**	**LM**	**U**	**Total**
Classification data	**DW**	**4**	0	0	0	0	0	0	0	0	0	4
	MW	2	**17**	1	0	0	0	0	0	0	0	20
	LW	0	0	**8**	0	0	0	0	1	0	0	9
	LO	0	0	0	**2**	0	0	0	0	0	0	2
	SO	0	0	0	5	**13**	0	0	0	1	0	19
	FC	0	0	0	0	1	**0**	0	0	0	0	1
	FG	0	0	0	4	3	1	**7**	0	1	0	16
	DM	0	0	0	0	2	0	1	**4**	0	0	7
	LM	0	0	0	8	13	1	0	0	**7**	0	29
	U	3	1	1	2	2	1	0	2	2	**0**	14
	Total	9	18	10	21	34	3	8	7	11	0	*121*

Total of the major diagonal = 4 + 17 + 8 + 2 + 13 + 0 + 7 + 4 + 7 + 0 = 62

Overall Accuracy = 62/121 = 0.512 x 100 = 51%

Producer's Accuracy
DW = 4/9 x 100 = 44%
MW = 17/18 x 100 = 94%
LW = 8/10 x 100 = 80%
LO = 2/21 x 100 = 10%
SO = 13/34 x 100 = 38%
FC = 0/3 x 100 = 0%
FG = 7/8 x 100 = 88%
DM = 4/7 x 100 = 57%
LM = 7/11 x 100 = 64%

User's Accuracy
DW= 4/4 x 100 = 100%
MW = 17/20 x 100 = 85%
LW = 8/9 x 100 = 89%
LO = 2/2 x 100 = 100%
SO = 13/19 x 100 = 68%
FC = 0/1 x 100 = 0%
FG = 7/16 x 100 = 44%
DM = 4/7 x 100 = 57%
LM = 7/29 x 100 = 24%

C. Calculations for the Two Class Test

		Reference data			
Classification data		**water**	**gear**	**unclassed**	**total**
	water	**32**	1	0	33
	gear	0	**74**	0	74
	unclassed	5	9	**0**	14
	total	37	84	0	*121*

Total of the major diagonal = 32 + 74 + 0 = 106

Overall Accuracy = 106/121 = 0.876 x 100 = 88%

Producer's Accuracy
water = 32/37 x 100 = 86%
gear = 74/84 x 100 = 88%

User's Accuracy
water = 32/33 x 100 = 97%
gear = 74/74 x 100 = 100%

The numbers in this table were produced from the nine-class test table; the actual classification was not run.